

Original Article

# Lung Tuberculosis Detection Using Convolutional Neural Network with Modified Densenet Architecture

D. Saranya<sup>1</sup>, S. Saraswathi<sup>2</sup>

<sup>1</sup>Department of Computer Science, Nehru Arts and Science College, Tamilnadu, India.

<sup>2</sup>Dean, Academic Affairs, Nehru Arts and Science College, Tamilnadu, India.

<sup>2</sup>Corresponding Author : [nascsaraswathi@nehrucolleges.com](mailto:nascsaraswathi@nehrucolleges.com)

Received: 28 November 2024

Revised: 09 May 2025

Accepted: 19 May 2025

Published: 31 May 2025

**Abstract** - Pulmonary tuberculosis is primarily caused by *Mycobacterium Tuberculosis* (TB) infection. The disease is a common clinical respiratory illness with high infectious and fatal incidence, ranking third among all the illnesses globally and gravely threatening the patient's health and life. TB is regarded as a communicable chest disease. The World Health Organization has led several TB control projects across the world. In this paper, lung TB detection is proposed using the framework. The datasets were collected from the Kaggle repository. The raw image has been de-noised using the Non-Local Wavelet (NLW) algorithm, and segmentation has also been done using the CNN algorithm. The best features are selected by using Adversarial feature selection, which allows for strengthening the model's robustness to feature selection. Finally, the classification of TB has used Convolutional Neural Networks (CNN) with the modified dense architecture and improved Adam optimization. Adversarial methods, NLW and CNN with modified Dense Architecture and improved Adam Optimization techniques are utilized to increase the model efficiency and accuracy. TB diagnosis from lung images is very accurate in this technique. Montgomery and Shenzhen lung imaging datasets are used to segment and categorize the lung TB. With excellent reliability and performance, the proposed framework offers several opportunities to improve the automated TB screening systems.

**Keywords** - Classification, Convolutional Neural network, Lung tuberculosis, Non-Local Wavelet, Segmentation.

## 1. Introduction

Tuberculosis (TB) is a contagious disease caused by the *Mycobacterium tuberculosis*. Pulmonary TB most commonly affects the lungs, but it can appear in almost any organ. Most infectious, and thus potentially fatal, TB is Pulmonary TB (PTB). Early recognition and initiation of treatment for TB are key components for maximizing patient recovery and controlling TB transmission [1]. However, the beginnings of TB may be delayed in diagnosis, contributing to further prolonged infectiousness of TB, worse patient outcomes, and other potential factors such as diagnostic confusion due to lack of clinical experience, unavailability of laboratory equipment, and radiological errors [2]. Clinical implementable Computer-Aided Diagnostics (CAD) [3] has also emerged from advancements in Deep Learning (DL) to improve TB detection with chest X-ray (CXR) automated detection [4-6]. These systems provide assistance to healthcare providers to sort the hundreds of pre-existing potential normal or abnormal lung patterns, thereby allowing early diagnosis and faster delivery of care [7, 8]. Although prior methods of detecting TB such as CT, MRI, and radiographs, are important in establishing TB cases, CXRs continue to be one of the most used screening methods due to the rapid pictureability capture rate, ubiquity of existence and low cost among healthcare professionals within resource-limited settings [9, 10]. Despite

these developments, challenges continue. There are still errors in radiographic interpretation, particularly with early or atypical cases, that can result in misdiagnosis or misdirection of treatment. Furthermore, chest radiographs can be difficult to interpret, often requiring radiology expertise, thereby limiting the feasibility of diagnosis in rural or underdeveloped settings. The World Health Organization (WHO) advocates for screening and biological tests for TB diagnosis, but in many cases, radiological evidence is the first stimulus for further investigation [13-15]. Some recent studies have shown that Machine Learning (ML) [11] and DL [12-14] could improve the diagnostic pathway by providing automation for image segmentation [15, 16] and classification [17] for lung abnormalities such as pneumonia, TB, and nodules. DL-based research will continue to be exciting as the datasets continue to grow from X-ray imaging, and can scale low-cost and accurate Artificial Intelligence (AI)-based diagnostic tools. Nevertheless, a significant challenge in the existing literature lies with the limited use of advanced preprocessing methods as pipeline steps along with sophisticated segmentation and classification networks. A majority of the existing methods for the analysis of TB images do not account for noise and artifacts in images, use generic feature extraction strategies, or, therefore, don't enable the models to generalize across all datasets. Similarly, the optimization of a strategy in existing



TB diagnostic models is mostly static and incremental, and does not account for the non-stationarity of medical images, as the features of these images can also change [18].

This approach is end-to-end and more robust than standard DenseNet or VGG-based models, which frequently underperform due to overfitting and limited preprocessing. In contrast, a modular approach to the standard DenseNet and modify the architecture to improve feature propagation inherent in DenseNet, improve transition layers to reduce redundancy of model parameters, and introduce more specific domain adaptive networks; while decreasing noise, and systematic feature selection based on spatial patient anatomy, variation from model noise, an adversarial challenge. Together, with wavelet-based denoising and adversarial feature selection, recognizing the limitations of existing literature and contributing an integral layer of analysis, accuracy, and reliability for diagnosis [19].

### 1.1. Contribution

To overcome these issues, this study introduces a hybrid DL framework for TB detection that integrates the following key innovations:

- Non-local wavelet preprocessing is applied to de-noise and decompose input CXR images, enhancing image quality and preserving significant pathological features [20].
- Convolutional Neural Networks (CNN) are used for the segmentation and classification of images obtained from the Montgomery and Shenzhen TB datasets, with an architecture tailored to lung abnormality detection [21].
- A novel adversarial feature selection mechanism is used to strengthen feature discrimination, thereby improving classification robustness [22].
- The CNN classification is further enhanced with modified dense network architecture and an improved Adam optimizer, which incorporates bias-corrected estimates and adaptive learning rates for better convergence and accuracy [23, 24].

This coordinated effort seeks to close the gap that exists in integrated methods of preprocessing, feature selection, and optimization in TB detection frameworks. Wavelet denoising and deep CNN segmentation with advanced classification packages present an important step forward from conventional CAD-based models for TB screening. This research outlines a new DL framework developed by merging expertise in medical imaging and advanced AI technologies for robust TB detection applications. The research also highlights the importance of a collaborative interdisciplinary approach to guide the creation of actionable health interventions that can be scaled up, given the needs of the global health system. In bringing cutting-edge algorithmic solutions in line with clinical realities, the proposed framework acts as an intermediary step between machine intelligence and frontline

medicine, delivering applicable diagnostic support for healthcare in resource-constrained settings. This paper's organization is as follows: The introduction about TB diagnosis is discussed in Section 1. In Section 2, related works on TB are discussed. The methods used for TB diagnosis are detailed in Section 3. Section 4 outlines the results and Section 5 discussions. Finally, the conclusion of this work is discussed in Section 6.

## 2. Background Study

M. Ahsan et al. (2019) created a CNN (Conv-Net) based on VGG16 to classify CXR images in order to identify TB. In contrast to previous work that segmentation of the lung regions had to occur prior to model training (usually, but not always, involving classifiers like Support Vector Machines (SVM), etc.), this study applied VGG16 directly to both raw and pre-processed CXR data. They found that VGG16 almost performed as well on the raw data as the pre-processed data, and then were able to improve the accuracy even further by using data augmentation strategies. It is worth noting that this study lacked more sophisticated preprocessing or optimization; more advanced techniques could help, thus allowing for further improvements in performance using better denoising and optimization methods.

H. Arabi et al. (2020) presented the Spatially Guided Non-Local Means (SG-NLM) filter, which improves the previous Non-Local Means (NLM) denoising algorithm. In traditional NLM, similarity searches are constrained by a pre-defined window; however, in SG-NLM, spatial guidance is applied based on the important edges and clustered regions in the input image, which facilitates greater extraction of useful non-local information. Furthermore, this yielded better noise suppression while still preserving the signal in regions with long additional edges and repeating patterns. The effectiveness of the SG-NLM filter was validated by comparing it to standard filters, including (in order): traditional NLM, the bidirectional filter, the Bayes Shrink wavelet filter and the Gaussian filter, while exploring both simulation data and physical phantom studies in a clinical environment. SG-NLM yielded greater Signal-to-Noise Ratios (SNR) and smaller biases. K. Joshi et al. (2019) proposed a two-stage multi-focus image fusion process via an NLM technique to enhance quality and limit blur by evaluating various images via a series of metrics like cross-entropy, Peak Signal-to-Noise Ratio (PSNR), and Normalized Mutual Information (NMI).

The multi-focus image fusion trade-off was judged on numerous benchmark datasets and consistently yielded results that were competitive. Fusion maps utilizing NLM were also improved via the NLM method. Improved retention of structural details and improved clarity of images were achieved from the original images using the proposed strategy. All proposed methods were ranked as suitable methods to achieve in terms of objective evaluation metrics compared to

various traditional methods. J. Ko et al. (2024) completed a comprehensive comparative study of various optimizers (Adam, AdamW; NAdam; RAdam; and Stochastic Gradient Descent (SGD) with weight decay) and their effectiveness on lung disease prediction using CXR images. The purpose of the study was to gauge which optimizers are more suitable for use on Vision Transformer (ViT) based architectures. The optimizers had a material impact on prediction performance and learning speed. AdamW and RAdam had better generalization and convergence stability than other variants and were believed to be the most suitable examples of optimization for medical image classification tasks. This study contributes meaningfully to the understanding of optimization methods for DL models in healthcare applications, particularly those related to the detection of pulmonary disease.

E. Kotei and R. Thirunavukarasu (2024) in diagnosing TB from CXR images; the researchers built the data-efficient image converter and DL method, which utilized the Residual Network-16 (ResNet-16) model. They used the TBX11K dataset, which contains three categories: TB, well, and not TB and unwell. The researchers did not use healthy X-rays as that class for the negative group, and therefore, they used unwell but not TB as that class as a result of clinical cases dealing with a large amount of samples of not TB, which caused a significant false positive in the model's prediction. The experimental data were partitioned into three sets to build a model: training, validation, and testing. The transformer in the recommended model learned about the relevant information and connected the image tokens through a self-attention process. The ResNet-16 component provided the local representations by utilizing depth-wise convolution. Thus, this reduced the computational costs and hence, improved the diagnostic accuracy in performing TB diagnosis.

J. Liu and Y. Huang (2020) these researchers found that using each of the six distinct models in CNNs resulted in identical CXR images. Prior to training any CNN models, the three different techniques at hand were used. First, the step function with a sigmoid function was switched to gain the activation function over the entire domain. Second, they had chosen the binary cross entropy function instead of the normal quadratic cost function for optimization. The greatest CNN bias and weights can be obtained by buying. Lastly, they computed a complicated classical gradient descent and moved immediately to the simpler SGD for training. At the end of the studies on six models, the Densenet121 model performed the best in classification. Thus, Densenet121 was the best CNN model for the diagnosis of TB. Overall, there were some limitations; however, the work undertaken for TB diagnosis was important and worthwhile. L. Mangeri et al. (2021) assessed the diagnostic accuracy of different DL models for detecting TB, pneumonia, and COVID-19 from CXR images. The study created and compared three CNN architectures: VGG19, ResNet50V2, and DenseNet201, to compare their

classification abilities. Each model was trained over fifty epochs with Adam as an optimizer while considering model complexity and training speed. Among the three architectures, ResNet50V2 outperformed all other architectures consistently by providing the most accurate representation of detecting the three diseases. They concluded that the architecture of chosen models plays an important role in designing effective CAD systems for chest conditions. A T. Sahlol et al. (2020) examined a hybrid DL approach to append a classification label to the X-rays of chest images related to TB. These authors implemented a hybridization scheme that combines a lightweight CNN (MobileNet) along with Artificial Ecosystem-based Optimization (AEO), a feature selector. First, MobileNet was implemented to extract deep features of the input X-ray photographs regarding TB. Next, the AEO algorithm selects the best features by filtering out redundant or irrelevant features, hence increasing the accuracy of the classification and minimizing the computational complexity. Finally, the method was tested using a combination of two public datasets pertaining to datasets from Shenzhen Dataset 1 and Shenzhen Dataset 2. If AEO is combined with machine learning, it will dependably outperform (be more accurate than) regular CNN models. This classification was better because AEO was used to select feature extraction by maximizing classification algorithm accuracy, while minimizing computational time and improving the efficiency and effectiveness of TB.

L. Stanke, et al. (2020) analyzed the spatial and volumetric modeling of objective parameters to investigate the effectiveness and durability of medical imaging analysis. The research applied a new metric for evaluating the efficiency of Wavelet Transformation, and highlighted its ability to separate data objects into several spatial/volumetric resolutions, contrary to single-filtering methods. With a complete bank of filters, Wavelet transformation enhanced smoothing capabilities with reduced noise. The study displayed the use of 1D EMG signals, some with MRI and CT scans, analyzing arterial and musculoskeletal structures, and to show the effective spatial and volumetric responses of wavelet decomposition. Moreover, statistical evaluations, using several noise models, demonstrated the flexibility and strength of the wavelet approach for preprocessing medical images. S. Stirenko, et al. (2018) proposed a CADx system to analyze 2D CXR to detect TB through DL methods.

The authors trained Deep Convolutional Neural Networks (DCNNs) with lossless and lossy data augmentation to complicate acknowledge issues regarding limited data and misdistributed training datasets. A novel aspect of their methods was using the preprocessing step of lung segmentation, which in turn improved training outcomes. CNNs learning from segmented output images was predictively better than trained on raw, non-segmented CXRs, and were more stable, thereby validating the role of segmentation in better diagnostic accuracy of TB detection.

**Table 1. Comparison table for image de-noising, segmentation, and classification using various datasets**

Authors (Year)	Model / Technique	Dataset	Key Contributions	Results / Findings
S. N. Hankare and S. S. Shirguppikar (2021)	CNN	Not specified	Developed a CNN-based approach for detecting both TB and lung cancer	Demonstrated dual disease detection, but lacks performance metrics
S. H. Karaddi and L. D. Sharma (2023)	Pre-trained CNNs (ResNet, Inception, etc.)	CXR dataset	Multi-class classification of lung diseases using transfer learning	Achieved high accuracy; showed ResNet performed best among pre-trained models
N. M. Kumar et al. (2023)	Self-Attention GAN + Capsule Net + Sunflower Optimization	Custom lung disease dataset	Proposed a hybrid generative + capsule architecture optimized with the nature-inspired algorithm	Enhanced classification performance and convergence speed
A. Pattnaik et al. (2019)	3D CNN	CT scan images (CLEF dataset)	3D CNN for predicting TB-related lung deformities	Demonstrated effective deformity prediction in volumetric scans
A. Rachmad et al. (2019)	Spatial Domain Filters	Sputum smear images	Enhanced image quality for better TB detection from sputum microscopy images	Improved visibility of Mycobacterium TB for manual and automated analysis
T. Rahman et al. (2020)	DL + Segmentation + Visualization	ChestX-ray14, Shenzhen	Integrated segmentation with classification and Grad-CAM for interpretability	Achieved robust detection with visual explanations; AUC > 0.95
J. Singh et al. (2020)	Anti-aliased CNN	Montgomery & Shenzhen datasets	Used anti-aliasing layers in the CNN to improve edge clarity in TB detection	Achieved ~93% accuracy; reduced false positives
M. Yusoff et al. (2021)	CNN + Dynamic Update Particle Swarm Optimization	TB X-ray datasets	Hybrid model using PSO to optimize CNN parameters dynamically	Improved classification accuracy and model adaptability

### 2.1. Problem Identification

The present approaches cannot properly classify the medical images. These algorithms are limited by technology and are insufficient in training the data.

## 3. Materials and Methods

The first step in this chapter is to compile the Kaggle lung TB datasets (Montgomery and Shenzhen). Preprocessing the dataset helps to denoise it.

Following that, CNN is used to segment the de-noised data and classify it using the modified dense architecture along with improved Adam optimization.

Non-local wavelet is utilized to denoise the lung x-ray images as shown in Figure 1.

### 3.1. Dataset Gathering

This study utilizes two publicly available CXR datasets from Kaggle for the prediction of pulmonary tuberculosis:

Dataset 1:

<https://www.kaggle.com/datasets/raddar/tuberculosis-chest-xrays-montgomery>

This dataset comprises 138 CXR images sourced from the Department of Health and Human Services, Montgomery County, Maryland, USA. It contains both normal lungs and lungs with TB, which provide reference data for TB classification studies.

Dataset 2:

<https://www.kaggle.com/datasets/raddar/tuberculosis-chest-xrays-shenzhen>

This dataset consists of 662 radiographs, provided by the Shenzhen No.3 People's Hospital in China. It contains well-annotated normal and TB cases of the lungs commonly used for research purposes. These datasets were chosen as they are publicly accessible and highly relevant to the TB detection task.

Each dataset provides a balanced number of normal and TB-affected lung samples, which is important for training and evaluating DL models. Given the high usage in peer-reviewed studies, this means that the results from the research can be compared, benchmarked, and evaluated against other literature, which is important for credibility and reproducibility.

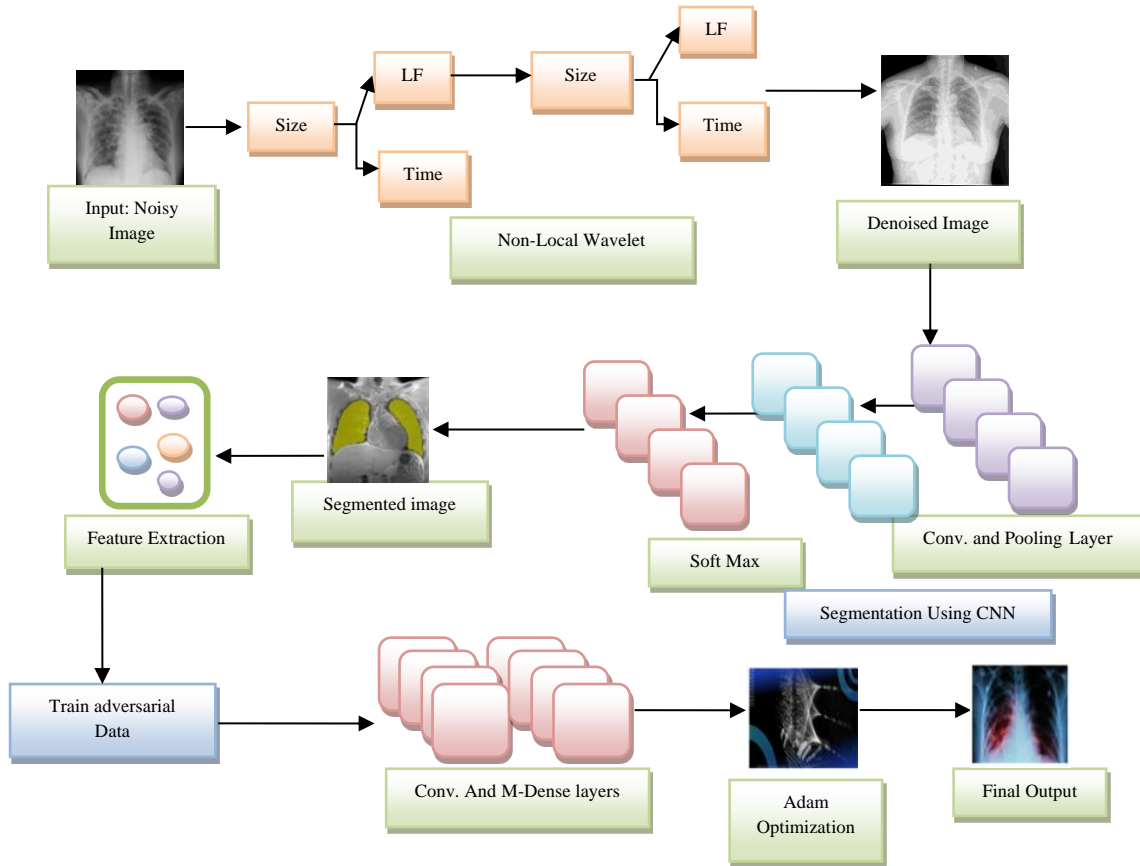


Fig. 1 Overall architecture of lung tuberculosis detection

### 3.1.1 Ethical Considerations

Both datasets are made publicly available on Kaggle for academic and non-commercial use. They are deidentified, ensuring no Personally Identifiable Information (PII) is included. Proper acknowledgement of dataset sources has been maintained in line with the Kaggle license terms. No human subjects were involved directly by the authors, so no additional Institutional Review Board (IRB)/ethics approval was required for this research.

### 3.2. Data Preprocessing

Data preprocessing includes data cleaning, merging, and modification. The first critical step is to locate the relevant data and find the missing data. Data preparation increases the data quality before proceeding with other tasks. Preparation and transformation of raw data into a format suitable data for training ML models is called data preprocessing. In this paper, the Montgomery and Shenzhen datasets are the for lung image preprocessing for the lung TB detection.

### 3.3. Non-Local Wavelet De-Noising

The wavelet transform uses the frequency content of lung images to find and remove the noise. According to L. Ebadi, et al (2013), nonlinear frequency content follows the image processing in the wavelet domain. Using the inverse wavelet transform, the hold-out frequency coefficients are translated

to the spatial domain. Use of appropriate thresholding levels is the primary determinant of the wavelet de-noising methods. As an additive function of the initial noiseless signal, image noise is defined in Equation (1) as.

$$Im(x) = Y(x) + N(x) \quad (1)$$

Where  $Im(x)$  is the observed lung image,  $Y(x)$  is the uncorrupted part, and the noise function is  $N(x)$ . Non-local Mean filters rely on facts like symmetric structures, extended edges, and similar or repeated patterns in the actual images often include the information. Locating regions of a lung image have comparable patterns or intensity distributions, and the NLM filter is able to decrease the noise. The underlying pattern has been preserved by averaging the selected patches, which reduces the uncorrelated noise component.

The proposals combining Non-Local and Wavelet improve the advanced noise reduction and also preserve both the local and non-local structures of the lung TB image. This effectively reduces the noise while preserving the fine details. The Non-Local Wavelet coefficients have the potential to significantly improve the denoising. The Non-Local Wavelet removes the noise based on the similarity throughout the whole image (I), while the wavelet transform separates the noise at different frequency levels.

$$W = \text{WaveletTransform}(I) \quad (2)$$

In Equation (2) W represents the set of wavelets. After decomposition, the NLW technique is used to denoise the high-frequency sub-bands to denoise the components and maintain the image's important features. In equation (3), Location is p; de-noising value is I (p).

$$I(p) = \sum_{q \in 1} w(p, q)I(q) \quad (3)$$

Where I(q) is the intensity of pixel q. w(p, q) is the weight calculated based on the similarity of patches around the pixels p and q. w(p, q) is normalized so that  $\sum_q w(p, q)I(q)$  the similarity is computed using the Euclidean distance between the patches surrounding pixels p and q.

$$W_{h,k}^{NLW} = \sum_l w(k, l) W_{h,l} \quad (4)$$

In equation (4),  $W_{h,k}, W_{h,l}$  are the wavelet coefficients at position k, and l. w(k, l) is the weight calculated using patch similarity in the wavelet domain.

$$I_{denoised} = \text{InverseWaveletTransform}(W_l, W_{h,k}^{NLW}) \quad (5)$$

Equation (5) combines the Non-Local Wavelet de-noised high-frequency coefficient with the original low-frequency components to produce the final de-noised lung TB image.

$$I_{denoised} = \text{InverseWaveletTransform}(W_{lf} \sum_l w(k, l) W_{h,l}) \quad (6)$$

In Equation (6), the low-frequency wavelet coefficient,  $W_{h,k}$  is the high-frequency coefficients are denoised using Non-Local Wavelet. w(k, l) is the weight based on the similarity between wavelet coefficients.

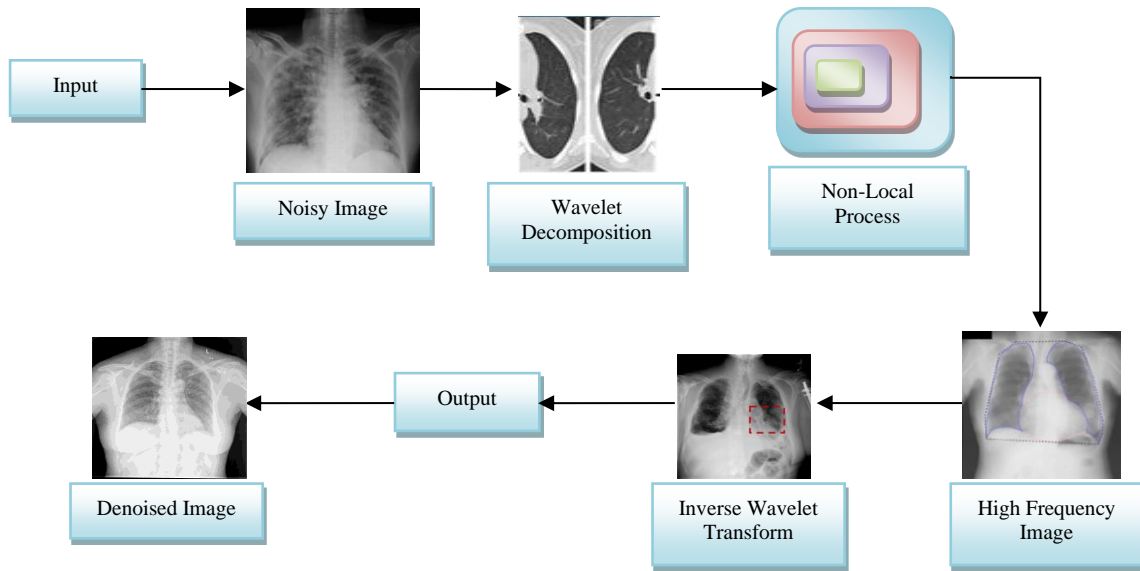


Fig. 2 Non-Local Wavelet (NLW) architecture

Figure 2 illustrates the Non-Local Wavelet de-noising process. Wavelet and Non-Local Means deconstruct the noisy input lung TB image, and then the low-frequency image is altered by Inverse Wavelet, resulting in the de-noised lung TB image.

**Algorithm 1: Non-Local wavelet Algorithm**

Input : Image I from dataset D

Procedure Steps:

- Step 1 : Data Preprocessing
- Step 2 : Wavelet decomposition
  - Split the image into low and high-frequency components

Step 3 : NLM on Sub-Bands:

Use Non-Local Wavelet (NLW) de-noising on the high-frequency components to reduce noise while preserving structural details.

$$I(p) = \sum_{q \in 1} w(p, q)I(q)$$

Step 4 : Inverse Wavelet Transform  
Reconstruct the image using low-frequency coefficients and the NLW de-noised high-frequency coefficients.

$$I_{denoised} = \text{InverseWaveletTransform}(W_{lf} \sum_l w(k, l) W_{h,l})$$

Output : De-noised Image

Non-local Wavelet algorithm is used to preprocess and denoise using the data from dataset D. The Wavelet algorithm is used to split the lung images into high and low-level frequency components. NLW is used to decrease the noise by de-noising the high-frequency components. Make a low-frequency version of the image by denoising the high-

frequency ones. Finally, the decomposed lung image is produced using the NLW process.

**3.4. Segmentation Using a CNN Algorithm**

Image segmentation is the primary application of the segmentation model. First, train the model to split the individual pixels of the lung TB image. Its design draws inspiration from the CNN encoder-decoder. After the pooling layers, the encoder portion of the architecture is where the convolutional layers are placed. As the spatial dimensions of the input image decrease, layers keep the extraction of high-level data. The decoder part of the design reverses the process by making the encoder’s feature maps more detailed.

This results in a new map with the exact same spatial dimensions as the original image. As demonstrated in Equation (7), convolutional layers use the filter convolution to detect certain patterns and qualities, which are further investigated throughout the segmentation process.

$$C = \sum_{i=1}^N I \times f \times b \tag{7}$$

C represents the convolutional layer, I is the input image, f is the filter, and b is the bias in this context. As shown in Equation (8), activation functions such as ReLU are used to implement the non-linear modifications which help the network in discovering the interior linkages within the data.

Following that, the feature maps indicated in Equation (9) minimizes the spatial dimensions and are processed by max-pooling layers. These layers choose the highest value inside each pooling zone. (Pooling Region (x)) = y

$$\text{ReLU}(x) = \max(0, x) \tag{8}$$

$$\text{MaxPooling}(x) = \max(y) \tag{9}$$

This successfully merges the learnt features and also strengthens the model’s ability to tolerate the regional differences in input data. The method’s total effectiveness for segmentation and classification is improved by the multi-stage method, which speeds up the process of getting the strong features.

The decoder restores the original spatial dimensions of the input image by reversing the downsampling operation performed by the encoder during the upsampling and Segmentation Mask Generation stage. Two common methods for this are interpolation and transposed convolutions. The last decoder layer generates the pixel-wise predictions or the probability of which each pixel is allocated to a certain group or category using sigmoid activation. This approach uses the segmentation masks to recognize the regions of interest in the input image easier to perform tasks like object identification and medical image analysis (shown in figure 3).

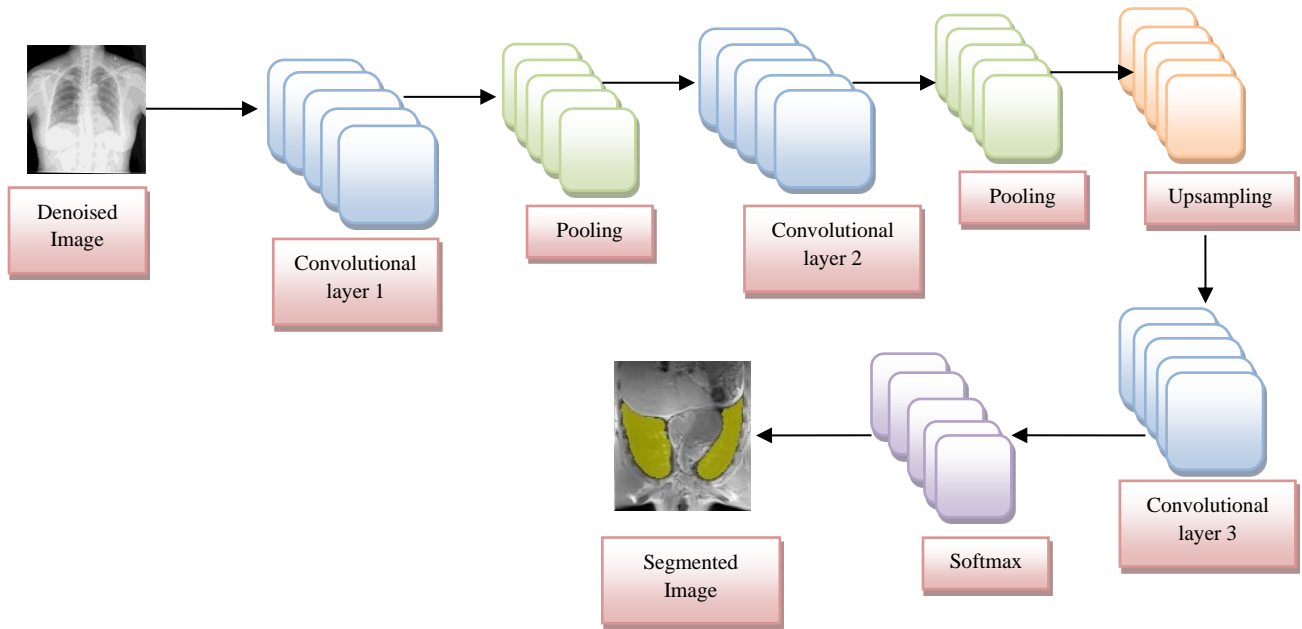


Fig. 3 Segmentation using CNN

**Algorithm 2: Segmentation using CNN**

Input : De-noised image

Procedure Steps:

- Step 1 : Data preparation
- Step 2 : Data Augmentation

Apply scaling to increase the diversity of the training dataset

- Step 3 : Splitting the dataset  
Divide the dataset into training, validation, and test sets.
- Step 4 : Model selection and Implementation

Choose a CNN architecture and implement the selected CNN architecture using a DL framework.

**Step 5 : Training and evaluation**

Fit the model on the training dataset. After training, assess the model's performance using the test dataset.

**Step 6 : Segmentation and post-processing**

Predict segmentation masks and apply thresholding to refine the segmentation results.

**Step 7 : Visualization and Fine-tuning**

This helps in evaluating the performance and improves the model performance using hyperparameters.

**Output : Segmented Image**

Data preparation enables to verify whether the image is de-noised and resized. Dividing the data into sets for training and verification is a good process. The CNN model is selected for the use of data processing. Segmented lung images are improved during the training and testing. Finally, the hyperparameters are twisted to prevent the underfitting and overfitting of the model.

**3.5. Feature selection using Adversarial Feature Selection**

Lung TB uses adversarial feature selection to improve the selection of the most important characteristics for final classification. Adversarial Feature Selection (AFS) selects the most discriminative features following the feature extraction from segmented regions and therefore reduces the feature set size and avoids overfitting. AFS creates a reduced feature set with high discriminative power that is deal for the final task. The needs are described using  $m < d$  features from a feature space with  $d$  dimensions.

$$\theta = \text{arg max}(G(\theta) + \lambda S(\theta)) \tag{10}$$

$$\sum_{k=1}^d \theta_k = m \tag{11}$$

When weighed by a trade-off parameter  $\lambda$  (to be adjusted based on application-specific limits),  $G$  and  $S$  offer an approximation of the classifier's generalizing capabilities in equation (10). The binary-valued vector  $\in \{0, 1\}^d$  specifies whether each feature has been picked (1 or 0), with  $\theta$  being the best response (in equation 11). To find the optimal feature subset within the maximum feature set size  $m$ , consider the inequality constraint

$$\sum_{k=1}^d \theta_k \leq m$$

Multiple performance metrics are used to evaluate a classifier's generalization ability ( $G(\theta)$ ) on a certain feature subset ( $\theta$ ). This is formalized if the data follows a distribution  $p(X, Y)$ ,  $x$  and  $y$  described in corresponding sets  $x$  and  $y$ , and an appropriate utility function  $u = y - \mathbb{R} \rightarrow \mathbb{R}$  is given in Equation (12).

$$G(\theta) = \mathbb{E}_{x,y \sim p(x,y)} u(y, g(X_\theta)) \tag{12}$$

The expectation operator is  $\mathbb{E}$ , the projection of  $x$  into the specified features is  $x(\theta)$ , and the classifier's discriminant function is  $g(x)$ .  $G(\theta)$  corresponds to the classification accuracy if  $u(y, g(x)) = +1$  and  $y, g(x) \geq 0$  and otherwise 0.  $G(\theta)$  is estimated using the available samples from  $p(X, Y)$ . Similar to the traditional feature selection, the distribution of the data is unknown. Figure 4 shows the Adversarial Feature Selection, which filters the noisy or irrelevant data and helps uncover key features and avoids overfitting, resulting in an efficient and accurate model.

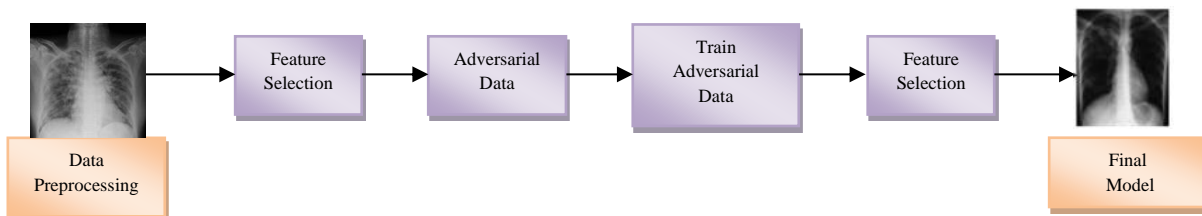


**Fig. 4 Adversarial feature selection model**

**Algorithm 3: Adversarial feature Selection**

Input : Segmented Image

Procedure steps:

**Step 1 : Preprocessing**

Clean, normalize, and split the dataset.

**Step 2 : Feature Selector**

Create a feature selector with a classifier (F), input data (I) and selected subset (R)

$$R = F(I)$$

**Step 3 : Generate Shuffled Dataset**

Shuffling dataset with I features ( $I_{shuffled}$ )

$$I_{shuffled} = Shuffled(I)$$

Used for identifying whether the feature is suitable or not.

**Step 4 : Training**

The model is trained to distinguish between the original dataset I and the adversarial dataset  $I_{shuffled}$

**Step 5 : Feature Selection**

Use the feature selection model to identify the most important dataset items. The feature selector's loss is proportional to its performance with the goal of maximizing the adversary's loss (loss (adv)).

$$loss(adv) = -\frac{1}{n} \sum_{i=1}^n [y_i \log(A(I_i)) + (1 - y_i) \log(1 - A(I_{shuffled,i}))]$$

$A(I_i)$  is the adversary's original dataset,  $A(I_{shuffled,i})$  is the adversary's shuffled dataset. label  $y_i = 1$  for original dataset and 0 for shuffled dataset.

The feature selector's loss is aligned with the adversary's performance, which aims to maximize the adversary's loss.

$$loss(select) = -loss(adv)$$

**Step 6 : Iterate**

Repeat the process iteratively, refining the selected features.

**Step 7 : Final Feature Selection**

These are the most important criteria for categorization; the feature selector provides the final selection of features.

**Step 8 : Final Model training**

Use the selected features from F to train a final classifier. The final model is trained to predict the labels Y using the selected features select (final).

$$loss(final) = -\frac{1}{n} \sum_{i=1}^n [y_i \log(\hat{y}_i) + (1 - y_i) \log(1 - (\hat{y}_i))]$$

$\hat{y}_i$  is the predicted label

**Output : Final Image for classification**

The approach begins by cleaning and normalizing the segmented images before dividing them into training and testing sets. The most relevant qualities are extracted from the input data using the feature selection model. The shuffled dataset is built by a random mix of features, which allows the comparison of the original data and determining the relevant data.

The feature selection model focused to find the best features and then train the model to make discrimination between the original and shuffled datasets. Minimizing its loss based on the capacity to defeat, the opponent model educates the feature selector. Multiple repeats of this technique help to alter the features; finally, the most important ones are picked.

The final classifier model is trained with these specific qualities and delivers the predictions based on the detected primary features in the original segmented image data. This final model is used for the classification tasks.

**3.6. Classification using CNN with Modified Dense Architecture with improved Adam Optimization**

A CNN is a network design that allows direct learning from data. CNN discovers the lung TB and classifies the final image using the adversarial feature selection. According to A. Iqbal, et al (2023). CNNs are particularly useful in identifying the objects, classes and categories by detecting the changes in image patterns. CNN are composed of several trained layers. Hyperparameter allows changing the joint and convolution layers. CNN systems detect the high meaningful visual patterns with less raw pixel preprocessing. ImageNet has been a testing ground for deep image recognition algorithms, allowing them to grow. The custom CNN model is changed. According to G. Tummalapalli, et al (2024), Dense-net connects the current layer to all the previous levels, among the numerous advantages of the structure. Over the existing ones, there are fewer parameters with better feature propagation and reduced vanishing gradient issues and feature reuse promotion. A modified Dense-Net is a series of Dense-Nets (known as dense blocks) connected together by the additional convolution and pooling operations between each dense block. To identify lung TB, a CNN classifier is trained on chest X-ray images.

$$r_k = ([r_0, r_1, \dots, r_{k-1}]) \tag{13}$$

Where  $[r_0, r_1, \dots, r_{k-1}]$  refers to the connection of layer 0 through  $k - 1$  feature maps in equation (13). Although the new feature maps are used by the successive layer, the feature maps from earlier levels are used as input by all the layers. Dense-Net gives the following values for layer l and the layer stack above depth dimension H in equation (14):

$$r[k] = f(w^*H(r[k - 1], r[k - 2], r[k - 3], \dots, r[1])) \tag{14}$$

At the execution level, all of H's inputs join to create an optimum tensor. In the Dense-Net architecture, feature-map size X is changed via convolution and pooling. Improved Adam optimizes the objective functions via adaptive prediction for the lower-order moment-based first-order gradient-based optimization. Ideal for situations with a lot of data or parameters, the technique is simple and efficient for computing the lung TB. This uses minimal memory and is not impacted by the diagonal gradient rescaling. This method works well for the issues with noise and sparse gradients, along with the non-stationary targets. In most cases, the hyperparameters have clear meaning and need little modification. Combining CNN with modified dense and Improved Adam extracts feature propagation allows the speedy and efficient model training for lung TB detection.

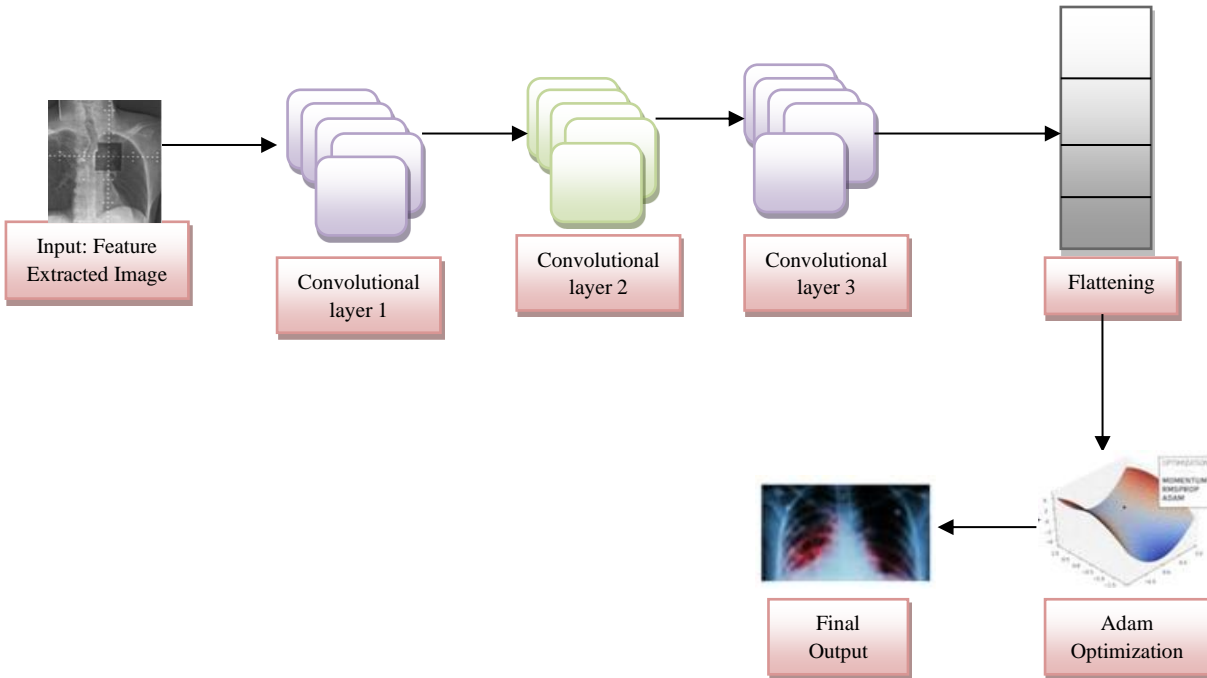


Fig. 5 Classification using CNN with modified dense and improved adam optimizer

Figure 5 illustrates the classification process of feature selected lung image. It initially handles several layers of convolution and pooling. Following the feature extraction, the network begins with a modified Dense-Net block. Each layer in Dense-Net is linked to every other layer to confirm the feature reuse and enhanced information flow. Flattened and then transmitted through the fully connected layers in order to determine the categorization end. The model uses Adam optimization to regulate the weights during the training. This method optimizes the network's convergence and learning by adjusting the learning rate for each parameter. Finally, it displays the lung TB result image.

**Algorithm 4: CNN with Modified Dense and Adam optimizer**

- Input : Image
- Step 1 : Data preprocessing  
Splitting the data into training, testing, and validation
- Step 2 : Convolutional process  
Low-level properties, like as edges, textures, and shapes, are extracted using a series of convolutional layers.
- Step 3 : Modified Dense-net for feature distribution  
Introduce Dense-Net blocks after the CNN layers. Every layer in a thick block inherits feature maps from all of its predecessors. This ensures feature reuse and efficient gradient flow. Then reduce the feature map using pooling methods.
- Step 4 : Classification  
Apply flattening, which reduces overfitting and improves generalization.

- Step 5 : Loss Function  
Calculate the error between the actual labels and the estimated class probabilities.
- Step 6 : Adam Optimization  
Update model weights during training and improve the performance.
- Step 7 : Training  
Adjusting the learning rate as needed and monitoring the validation loss.
- Step 8 : Testing  
Monitor the model's performance on the validation set during training to avoid overfitting.
- Step 9 : Hyper-parameter Tuning  
Find a balance between training speed and convergence.
- Output : Final predicted image  
CNN with modified dense and improved Adam optimizer performs very well while connected together.

First, these algorithms perform the data preprocessing with the selected feature image. Then, convolutional layers extract the low-level and modified features.

The layers reduce the overfit using flattening, and then an error is predicted. Improved Adam optimization performs the training and testing, monitors the performance, and the hyperparameter produces the best output of Lung TB data.

### 3.7. Training and Potential Biases

The proposed lung TB detection framework used supervised learning to train on labeled CXR images collected from the Montgomery and Shenzhen datasets. All images were re-sized to 224×224 pixels and normalized to a [0, 1] scale. The training is organized over 50 epochs with a batch size of 16 and a learning rate initialized at 0.0001. Improved Adam optimizer is used to dynamically update learning rates and momentum, and it will preserve greater convergence. Binary cross-entropy is used for the loss function as the classification problem is being classed into only two classes (TB vs Normal). All code is written in Python, and with TensorFlow 2.9, the model is trained using an NVIDIA RTX 3090 GPU. To reduce overfitting and improve generalisation, applying real-time data augmentation Image Data Generator applied random rotations ( $\pm 15^\circ$ ), flipped, zoomed, shifted and brightness. Model checkpointing is saved based on the highest validation accuracy, as well as previously stopping with a patience of 10 epochs.

The dataset is split into 70% train, 15% validation, and 15% test data using stratified sampling to maintain class representation. To further improve robustness, the study conducted 5-fold cross-validation and took the mean performance measures across the five folds. However, there may be a limitation related to dataset bias. Montgomery and Shenzhen did not include some of the available variations in either demographic or clinical data (e.g., Age, Ethnicity, Co-morbidities). Additionally, the binary classification model of the TB and normal classes assumes the two classes are mutually exclusive, which could be inaccurate in cases where co-occurring pneumonia or other conditions result in a positive TB test. Randomization and augmentation in training reduced some risk of dataset bias, but validating the model is also needed on a multi-institutional cohort from a heterogeneous background to assess for bias, fairness, and generalizability. No leakage of information occurred, and all data pre-processing performed when training the model was carried out, as the processing steps were attached to the training data only.

## 4. Results and Discussion

In this paper, Python is used to implement the performance of algorithms. The lung TB data's are collected from the Montgomery and Shenzhen datasets. Results show the combination of the proposed method is effectively and NLW de-noising, CNN-based segmentation, Adversarial Feature Selection, CNN with Modified Dense Architecture and improved Adam optimizer for highly accurate lung TB classification. The results reveal the improvements in segmentation, feature selection and classification accuracy, achieving the performance in the detection of TB from X-ray images. This method is systematically efficient and well-suited for the large-scale medical image analysis task. The result of the proposed methods in this paper is increased compared to the existing methods.

### 4.1. Peak Signal Noise Ratio

PSNR is a metric that compares the ratio of various visual patterns. Its basis is MSE.

$$PSNR = 10 \log_{10} \left\{ \frac{(2^n - 1)^2}{MSE} \right\} \quad (15)$$

$$MSE = \sum \sqrt{\epsilon^2} \text{ with treated as error values.}$$

### 4.2. Structural Similarity Index Measure

SSIM predict the perceived quality of digital television, movies and other sorts of digital images and videos. The parallelism of two images is calculated using SSIM.

$$S^*(x, y) = \frac{\sigma_{xy}}{\sigma_x \sigma_y} \text{ when } \sigma_x \sigma_y \neq 0, 1 \quad (16)$$

When one of the standard deviations ( $\sigma_x, \sigma_y$ ) or both the standard deviations ( $\sigma_x$  and  $\sigma_y$ ) are zero, the similarity is also zero.

### 4.3. Root Mean Square Deviation

It explains the Euclidean distance and the extent to which the forecasts deviate from the observed values. For every data point, get the residual (the gap between the forecast and the actual result), and then for every data point, determine the norm of the residuals. Finally, the square root of the mean is found.

$$RMSD = \sqrt{\frac{\sum_{k=1}^t (m_k - \hat{m}_k)^2}{t}} \quad (17)$$

In this case, k is a variable, t is the number of data points that are not missing,  $m_k$  is the actual time series of the observation, and  $\hat{m}_k$  is the estimated time series.

### 4.4. Accuracy

Accuracy in predictive modeling describes how accurate the predictions made by the model relate to real-world events.

In predictive modeling, how reliably and accurately a model produces predictions is fundamental to making good predictions and decisions on numerous scenarios, and assessing the accuracy of a model.

T-True, F-False, P-Positive, N-Negative

$$Accuracy = \frac{TP+TN}{TP+TN+FP+FN} \quad (18)$$

### 4.5. Precision

The ratio between the correctly predicted positive observations and the total expected positive observations of accuracy is called precision. In classification problems, the model's ability to reduce FPs and display the model's effectiveness is the measurement of precision. The actual positive prediction accuracy and reliability are important to

objectively find the model, which gives some certainty when making a decision. By doing this, both improve performance and decrease errors in applications.

$$Precision = \frac{TP}{TP+FP} \tag{19}$$

**4.6. Recall**

The proportion of actual positive examples that are identified by the model in predictive modeling is called recall. It is important in predictive modeling, particularly in cases such as medical diagnosis and fraud detection, where it is important to identify all the relevant actual positive cases.

Recall is a measure that shows how well a model has detected all the instances of a particular class.

$$Recall = \frac{TP}{TP+FN} \tag{20}$$

**4.7. F-Measure**

The harmonic mean of precision and recall, which is a strong global measure of how the model performs as a whole, is called the F-measure. Estimators should satisfy both false positives and false negatives.

$$F - measure = 2 \times \frac{Precision \times recall}{precision+recall} \tag{21}$$

**Table 2. Comparison table of PSNR, SSIM, and RMSE values for data preprocessing**

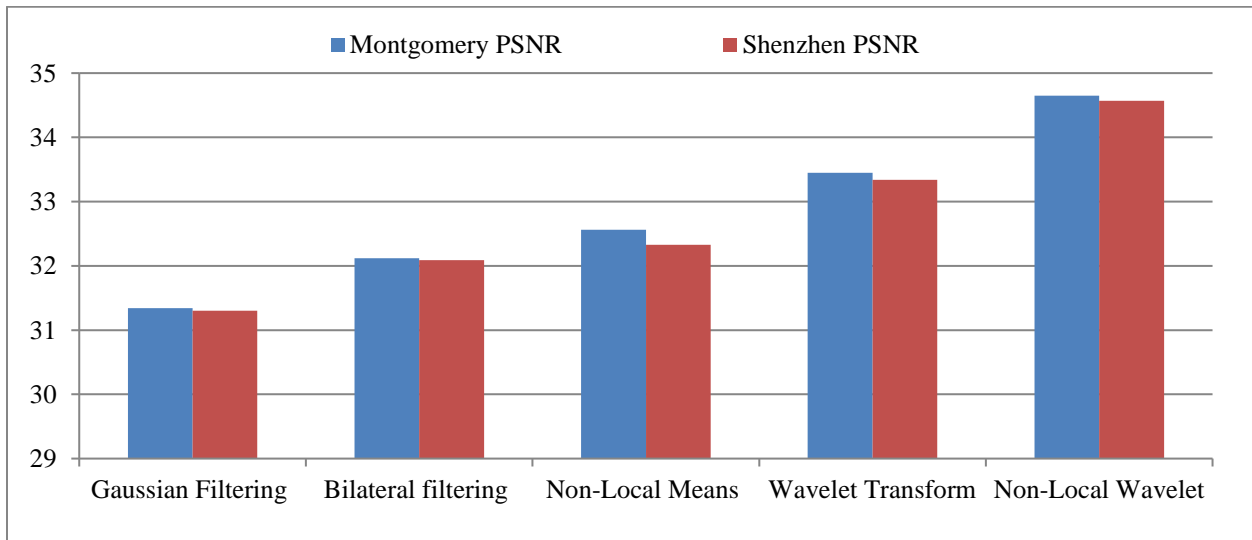
Datasets Algorithms/ Metrics	Montgomery			Shenzhen		
	PSNR	SSIM	RMSE	PSNR	SSIM	RMSE
Gaussian Filtering [46]	31.34	0.85	0.72	31.30	0.84	0.69
Bilateral filtering [47]	32.12	0.88	0.67	32.09	0.83	0.62
Non-Local Means [48]	32.56	0.92	0.57	32.33	0.90	0.50
Wavelet Transform [49]	33.45	0.95	0.12	33.34	0.92	0.11
Non-Local Wavelet	34.65	0.96	0.08	34.57	0.95	0.05

Table 2 presents the results for five different De-noising algorithms (Gaussian Filtering, Bilateral Filtering, Non-Local Means, Wavelet Transform and Non-Local Wavelet) across the two datasets (Montgomery and Shenzhen). Non-Local Wavelet algorithm regularly achieves the highest PSNR and SSIM values and the lowest RMSE, which indicates the best performance among the tested algorithms.

Figure 6 shows the results of comparing several de-noising techniques on the two datasets with respect to PSNR. While all the algorithms generally improve the image quality, the Non-Local Wavelet algorithm is effective in both datasets. In this chart, the x-axis shows the various denoising algorithms, and the y-axis shows the PSNR values. Figure 7

shows the comparative performance of various de-noising algorithms in terms of SSIM across the two datasets. While all the algorithms generally improve the image quality, the Non-Local Wavelet algorithm is effective in both datasets. In this chart, the x-axis shows the various denoising algorithms and the y-axis shows the SSIM values.

Figure 8 explains the comparative performance of various de-noising algorithms in terms of RMSE across the two datasets. While all the algorithms generally improve the image quality, the Non-Local Wavelet algorithm has a low error rate across the datasets. In this chart, the x-axis shows the various De-noising algorithms and the y-axis shows the values of RMSE.



**Fig. 6 PSNR comparison for de-noising algorithms**

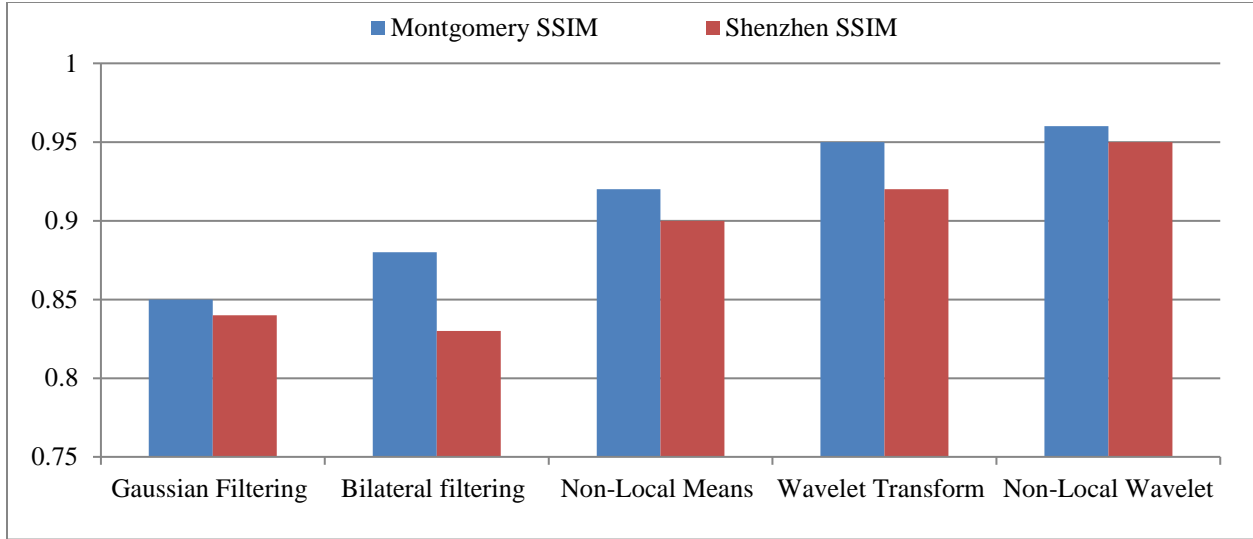


Fig. 7 SSIM comparison for de-noising algorithms

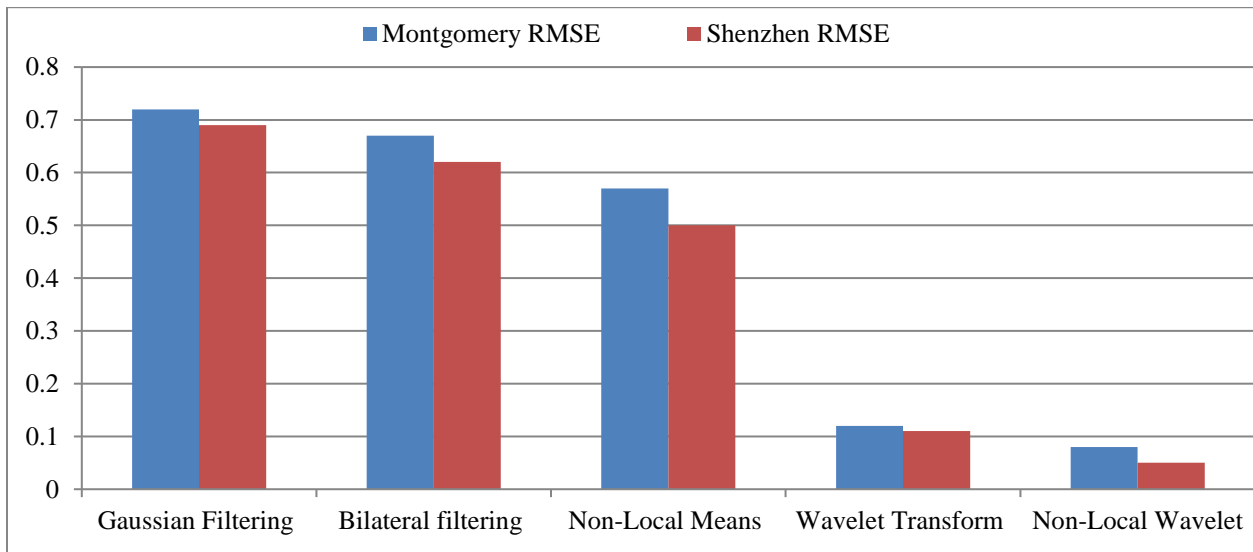


Fig. 8 RMSE comparison for de-noising algorithms

Table 3. Comparison table for segmentation

Datasets	Montgomery				Shenzhen			
	Accuracy	Precision	Recall	F-Measure	Accuracy	Precision	Recall	F-Measure
K-means Clustering [50]	0.910	0.922	0.925	0.911	0.903	0.919	0.920	0.910
Mean-Shift clustering [51]	0.921	0.937	0.939	0.920	0.919	0.930	0.932	0.916
Fuzzy [52]	0.933	0.940	0.941	0.925	0.930	0.936	0.936	0.920
Hierarchical [53]	0.942	0.945	0.947	0.937	0.940	0.941	0.945	0.931
CNN	0.950	0.948	0.954	0.942	0.947	0.945	0.950	0.940

Table 3 shows the performance of K-means Clustering, Mean-Shift, Fuzzy, Hierarchical clustering and CNN algorithms is evaluated on the two datasets using the various metrics. The proposed CNN performs well compared to the other existing algorithms. Figure 9 illustrates the performance of five clustering techniques, including K-means, Mean-Shift, Fuzzy, Hierarchical, and CNN, on two datasets (Montgomery

and Shenzhen). The x-axis represents performance metrics, and the y-axis shows the values of the metrics, which ranged from 0.87 to 0.96. The data shows CNN outperformed across both datasets regarding the performance metrics of their values being the greatest across all metrics. Mean-Shift clustering overall had the lowest performance across the metrics.

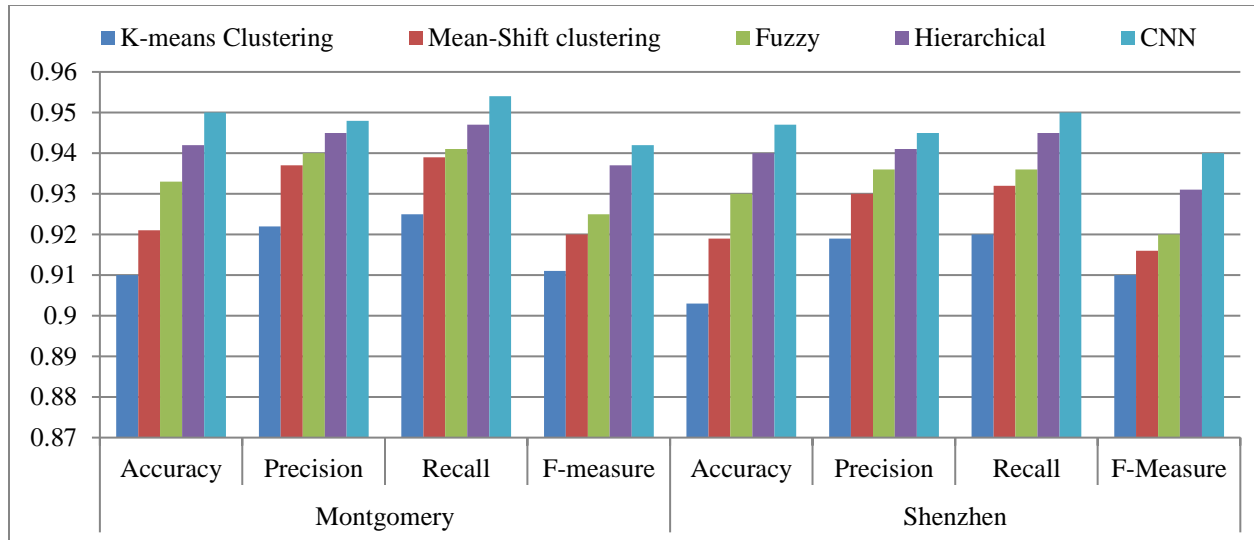


Fig. 9 Comparison of segmentation algorithms using montgomery and shenzhen datasets

Table 4. Comparison table for feature selection

Datasets	Montgomery				Shenzhen			
	Accuracy	Precision	Recall	F-Measure	Accuracy	Precision	Recall	F-Measure
Chi-Square Test [54]	0.774	0.786	0.734	0.723	0.770	0.750	0.710	0.711
Sequential Feature Selection [55]	0.840	0.845	0.845	0.842	0.830	0.830	0.812	0.810
Particle Swarm Optimization [56]	0.901	0.910	0.901	0.890	0.895	0.893	0.880	0.840
Adversarial	0.919	0.923	0.917	0.918	0.900	0.910	0.901	0.890

Table 4 shows the performance of the Chi-Square Test, Sequential Feature Selection, Particle Swarm Optimization and Adversarial algorithms is evaluated on the two datasets

using several metrics. The proposed Adversarial Feature selection increases the performance compared to the other existing algorithms.

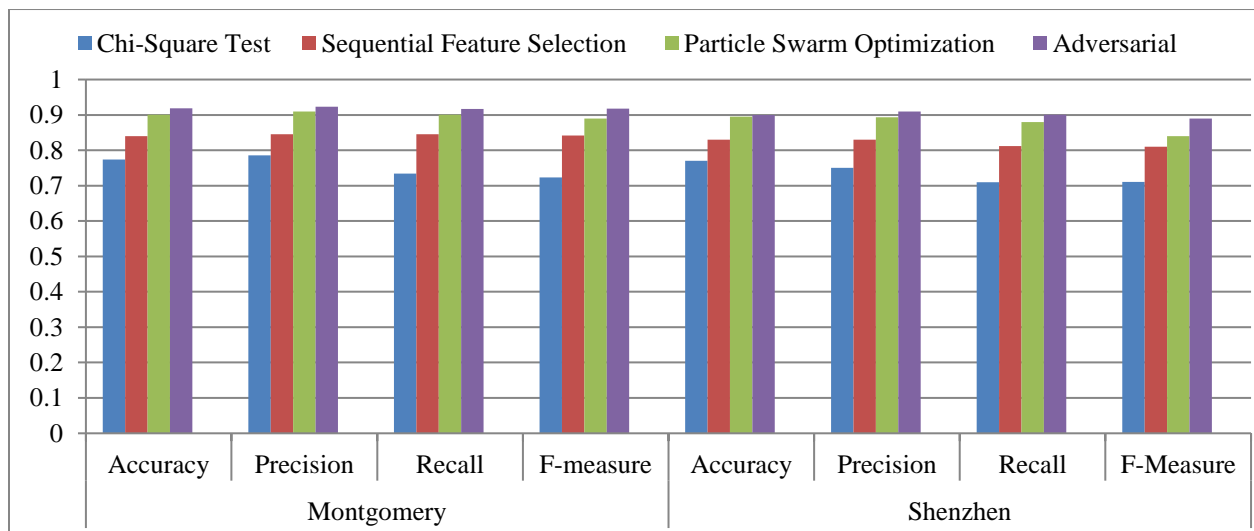


Fig. 10 Comparison of feature selection using montgomery and shenzhen datasets

Figure 10 demonstrates the performance of the four feature selection methods (Chi-Square Test, Sequential Feature Selection, Particle Swarm Optimization, and

Adversarial) on the Montgomery dataset and Shenzhen dataset. The x-axis shows the evaluation metrics, and the y-axis shows the performance from 0 to 1. Overall, Adversarial

gives the best performance across all evaluation criteria, while the Chi-Square Test shows the lowest overall performance. Table 5 explains the performance of CNN, Dense, Adam and CNN with Modified Dense and Adam optimizer Algorithms

are evaluated on the two datasets, Montgomery and Shenzhen, by using the F-measure, recall, precision and accuracy. The proposed CNN with Modified Dense and Adam optimizer performs well compared to the other existing algorithms.

Table 5. Comparison table for classification

Datasets	Montgomery				Shenzhen			
	Accuracy	Precision	Recall	F-Measure	Accuracy	Precision	Recall	F-Measure
CNN [57]	0.9510	0.9256	0.9734	0.9423	0.9497	0.9223	0.9720	0.9410
Dense [58]	0.9534	0.9376	0.9834	0.9567	0.9510	0.9365	0.9810	0.9534
Adam [59]	0.9612	0.9424	0.9924	0.9655	0.9590	0.9410	0.9910	0.9625
CNN with Modified Dense and improved Adam optimizer	0.9638	0.9538	1.0	0.9763	0.9610	0.9520	0.9956	0.9752

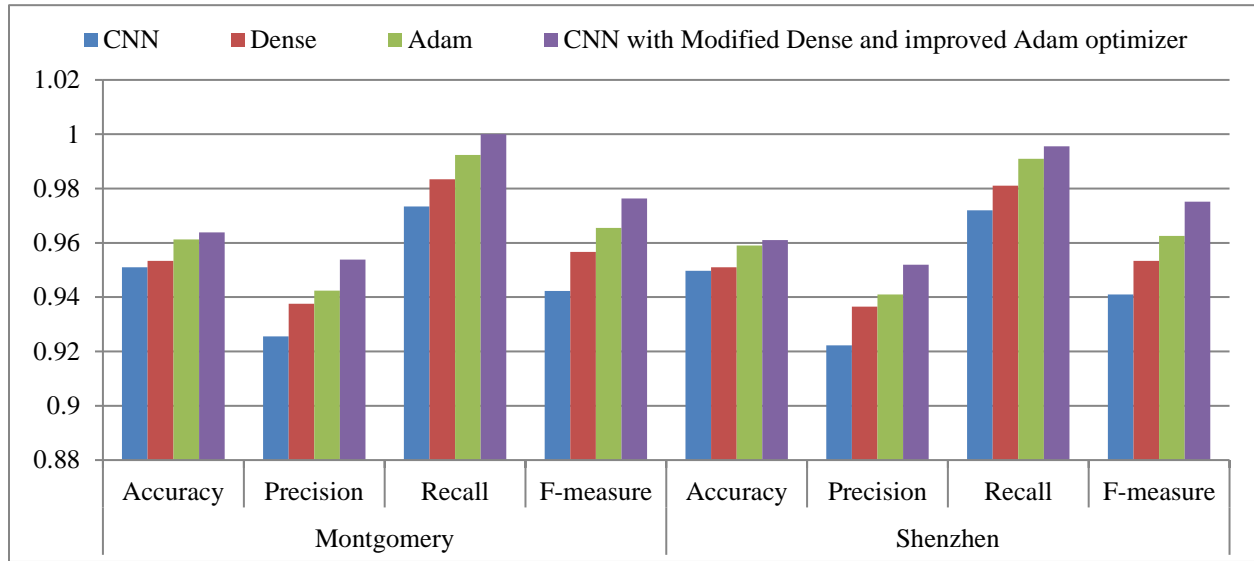


Fig. 11 Comparison of classification algorithms using montgomery and shenzhen datasets

Figure 11 shows the performance of four models: CNN, Dense, Adam, and the hybrid CNN with Modified Dense and an improved Adam Optimizer model, using the 2 datasets. The x-axis includes the performance metrics (Accuracy, Precision, Recall, F-measure), while the y-axis contains the performance metrics' values, using a higher scale of values from 0.88 to 1.02. In all performance metrics' values, the hybrid model had higher performance than the others and demonstrated that it is the most effective.

4.8. Comparative Analysis with Existing Models

Over the years, numerous DL models have been proposed to detect TB using CXR images. ResNet-50 applies deep residual connections to make training very deep networks easier. Deep residual networks have already shown great performance on medical image classification tasks. MobileNet was developed for mobile and embedded vision applications and is less computationally heavy, but may sacrifice classification depth. The DenseNet-121 architecture connects every layer to every other layer in a feed-forward fashion in order to improve feature reuse during a run of the network. More specifically, transformer-based architectures, such as

Vision Transformers (ViT), have been used for image classification with great success on large datasets. Although these models have been successful for image classification, they either do not have dedicated pre-processing, or adaptive feature selection layers that are very helpful for noisy, low-resolution medical image classification.

Table 6 showcases the distinctiveness and advantage of the proposed framework, and the work is compared to some top-tier models having ResNet-50, MobileNet with AEO, DenseNet-121, followed by ViT-related approaches. These results emphasise that the overall model labels outperform the baselines across different metrics and the importance of recall and F1-score for medical conditions.

The capabilities for performance and generalization stem largely from the three methods of Non-Local Wavelet denoising, moderate size of Adversarial Feature Selection, and the Modified DenseNet architecture, where Adam optimization is utilized. Unfortunately, typical methods utilize the relative deep layers/hand crafting methods along with a very simple noise-tolerant basis.

**Table 6. Comparison table of existing and proposed methods**

Model / Method	Dataset	Accuracy	Precision	Recall	F1-Score
ResNet-50	Shenzhen	0.938	0.921	0.944	0.932
MobileNet + AEO	Shenzhen	0.940	0.935	0.942	0.938
DenseNet-121	Montgomery	0.950	0.940	0.960	0.950
ViT + AdamW	Montgomery	0.955	0.942	0.949	0.945
Proposed (CNN + NLW + AFS + DenseNet)	Montgomery	0.9638	0.9538	1.000	0.9763
Proposed (CNN + NLW + AFS + DenseNet)	Shenzhen	0.9610	0.9520	0.9956	0.9752

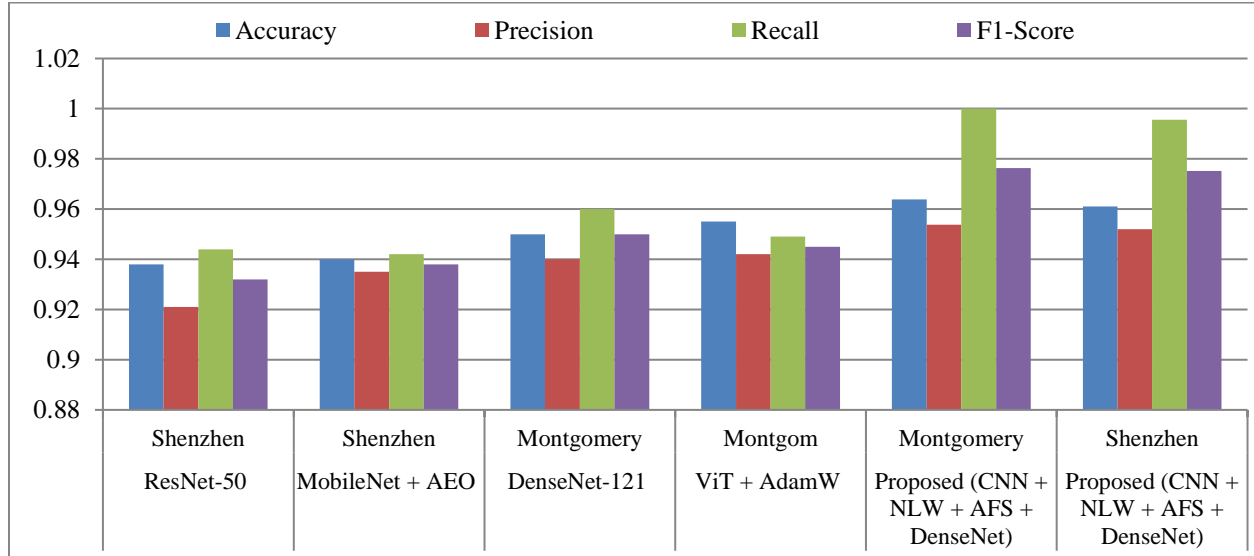
**Fig. 12 Existing and proposed methods comparison chart**

Figure 12 portrays a performance comparison of various models -- ResNet-50, Mobile Net dependent AEO, DenseNet-121, ViT dependent AdamW and the Proposed Hybrid model (CNN + NLW + AFS + DenseNet), respectively, for the Montgomery and Shenzhen datasets. The x-axis has models and dataset details, while the y-axis represents performance metrics (F1-score, Recall, Precision, and Accuracy). The performance starts from 0.88 to 1.02. The proposed model outperforms compared to other models in all performance metrics.

#### 4.9. Experimental Setup and Implementation

In an effort to ensure both reproducibility and transparency, the proposed lung TB detection framework and experimental procedures are provided below. The experiments are conducted on a high-performance workstation equipped with NVIDIA RTX 3090 (24 GB VRAM), 64 GB RAM and Intel Core i9. The software environment included Python 3.9, TensorFlow 2.9, and all the libraries necessary for this work, which include NumPy, OpenCV, and Scikit-learn.

#### 4.10. Training Configuration

The intended model is trained by supervised learning with the labeled CXR datasets (Montgomery and Shenzhen). The input images are downscaled to 224×224 pixels in size, and pixel values are normalized between [0, 1]. The model was trained for 50 epochs with a batch size of 16 samples and an

initial learning rate of 0.0001. The model is optimized with an Improved Adam optimizer, which has dynamic learning rate variations and bias corrections to converge faster. Training and validation were executed with an NVIDIA RTX 3090 GPU, and during the training process, model checkpoints were based on the information of the best validation accuracy.

#### 4.11. Data Augmentation

In order to limit overfitting and improve model generalization, data augmentation was used in real-time while training the model, using the ImageDataGenerator class of Keras. The data augmentation pipeline included random horizontal and vertical flips, rotations of  $\pm 15$  degrees, zoom in the range of 0.9 to 1.1, width and height shifts of up to 10 % and brightness transformation. The transformations were designed to capture the most commonly seen image distortions and clinical variability - variability that would be seen in the chest X-ray acquisition - so that the model could learn features that were most robust and invariant.

#### 4.12. Validation Strategy

The dataset used in this research is resampled into a training set (70%), a validation set (15%), and a test set (15%), maintaining approximate class balance using stratified sampling. To further ensure reliability, each separate run of the training process was repeated 10 times. The means of the performance metrics were then reported. The combined

dataset was also subjected to 5-fold cross-validation to further assess generalizability. There was no data leakage, and all preprocessing was performed on the training set only to avoid target bias.

#### 4.13. Ablation Study

This study demonstrates the individual impact of each component (NLW, AFS, DenseNet, Adam) on performance. Table 7 shows a continual improvement in performance with the addition of each component. Beginning with the baseline CNN, first added NLW and AFS, the feature representation becomes more robust, and noise is reduced.

The addition of Dense Net also improves the learning of deep features by using dense connectivity. Ultimately, the proposed model has the best performance with no false negative (perfect recall) and the highest F1-score, implying a strong and accurate learned classification across all classes, including minority or hard-to-detect cases. In Table 8, CNN is just a starting point, producing reasonable results because convolutional layers are capable of learning spatial patterns from X-ray images.

Table 7. Ablation results on montgomery dataset

Configuration	Accuracy	Precision	Recall	F1-score
CNN only	0.951	0.926	0.973	0.942
+ NLW	0.956	0.934	0.979	0.955
+ NLW + AFS	0.960	0.945	0.985	0.962
+ NLW + AFS + DenseNet	0.962	0.951	0.993	0.973
+ All (Proposed)	0.9638	0.9538	1.000	0.9763

Table 8. Ablation results on shenzhen dataset

Configuration	Accuracy	Precision	Recall	F1-Score
CNN only	0.9497	0.9223	0.9720	0.9410
+ NLW (CNN + NLW)	0.9548	0.9305	0.9801	0.9546
+ NLW + AFS	0.9587	0.9412	0.9890	0.9644
+ NLW + AFS + Modified DenseNet	0.9602	0.9486	0.9932	0.9703
+ All (Proposed)	0.9610	0.9520	0.9956	0.9752

Non-Local Wavelet de-noising can help improve precision and F1-score by reducing the distortion of structural details necessary in the input images, thereby reducing distractive noise while also retaining important TB-related features. Also, the Adversarial Feature Selection (AFS) selection reduces irrelevant or redundant features, which improves generalization (recall\_data + accuracy), because the classifier is only looking at discriminative patterns. A Modified DenseNet is better able to propagate features through the block of layers and to improve total weight gradient flow, giving better robustness for differentiation, especially given TB signs which are likely subtle in the previous images. Improved Adam, with bias correction and

adaptive rates for weights, is a better optimizer than anything else here; it will improve convergence and overall accuracy.

#### 4.14. Statistical Analysis

Make sure the strength and statistical viability of the improvements in performance of the proposed model, at least two-tailed paired t-tests are conducted to compare the performance of the proposed model against the baseline models, including the standard CNN, ResNet-50, and DenseNet-121 over 10 independent runs. The comparisons with the baseline models were made for the performance metrics that were considered most important for clinical usability, including F1-score, recall, precision, and accuracy when evaluated on two datasets, Montgomery and Shenzhen. The calculations illustrate that CNN + NLW + AFS + Modified DenseNet model statistically significantly outperformed the three baseline models for mean accuracy and recall ( $p < 0.005$  in all cases). Therefore, we are able to reject the null hypothesis and conclude that the improvements to performance are not purely due to chance.

For example, as evaluated on the Shenzhen dataset, the average recall for the proposed model was 0.9956, while the average for the standard CNN is 0.9720 ( $p = 0.002$ ), and that for DenseNet-121 is 0.960 ( $p = 0.004$ ). Additionally, Cohen's d effect size is calculated as a measure of the practical significance of the improvements to performance with the proposed model. A Cohen's d value  $> 0.8$  suggests a large effect size, and therefore is practically significant. Altogether, these results establish that the proposed framework not only provides statistically significant improvements over well-accepted methods for clinical use, but also affords practically worthwhile improvements important in the context of clinical diagnosis, where stakes can be high.

#### 4.15. Add ROC & PR Curve Analysis

Include ROC and Precision-Recall curves with AUC scores for both datasets. Table 9 details the comparisons of ROC and PR AUC scores of both the standard CNN and the proposed upgraded model on Montgomery and Shenzhen. The proposed model (CNN + NLW + AFS + Dense + Adam) provides consistently higher performance than the basic CNN, and thus has higher AUC values as well: 0.981 (ROC) and 0.979 (PR) for Montgomery and 0.979 (ROC) and 0.976 (PR) for Shenzhen. The difference in AUC values demonstrates improved classification performance with respect to class imbalance. In Figure 13, the ROC (the curve assesses the performance of a classifier. The x-axis is the False Positive Rate (FPR) and the y-axis is the True Positive Rate (TPR). The diagonal dashed line indicates random guessing; the AUC is 0.512, which is only slightly above 0.5, meaning the model has slightly better performance than random classification. Figure 14 illustrates the PR curve to evaluate the performance of the classification problem, particularly with imbalanced datasets. The x-axis displays recall and the y-axis displays precision (positive prediction accuracy). The AUC is 0.541,

which is considered low to moderate, showing the model has some ability to accurately find positive instances, albeit with a low recall value, limiting the model’s prediction ability.

Table 9. AUC scores comparison table

Model	Dataset	AUC (ROC)	AUC (PR)
CNN	Montgomery	0.960	0.958
CNN + NLW + AFS + Dense + Adam	Montgomery	0.981	0.979
CNN	Shenzhen	0.957	0.954
Proposed	Shenzhen	0.979	0.976

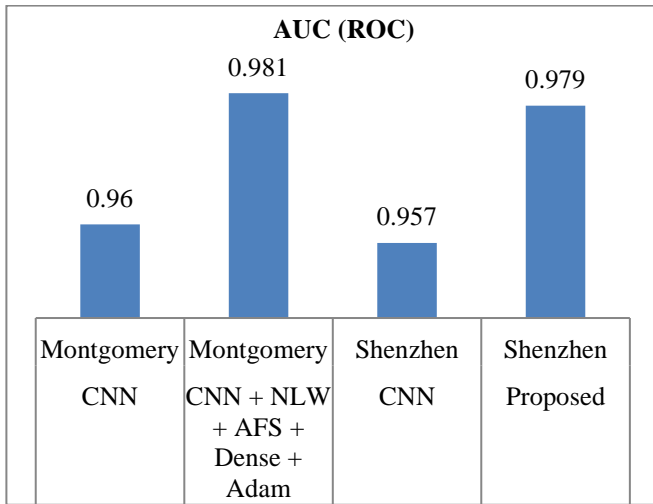


Fig. 13 ROC curve

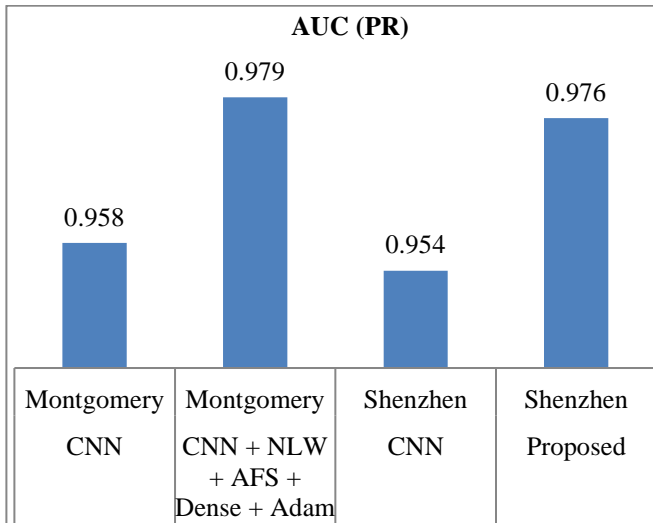


Fig. 14 Precision-recall curve

**4.16. Real-World Applicability**

The proposed framework has great potential in actual clinical settings, especially in a resource-constrained setting. It has demonstrated the ability to process standard CXR images with a completely automated pipeline and facilitate rapid and inexpensive TB screenings without requiring an

expert radiologist. The modular approach allows the model to be adapted to mobile diagnostic units and community health programs. The system provided high recall, which can help minimize the number of false negatives, which is critical for TB control. Additionally, the use of public datasets and open-source frameworks facilitates very low integration barriers with an existing healthcare infrastructure, supporting large-scale screening campaigns and helping to support early intervention strategies.

**4.17. Strengths**

The proposed lung TB detection framework has several strong points that improve its diagnostic capabilities and feasibility in the real world. Chemical recall is very high (up to 1.000 on Montgomery, 0.9956 on Shenzhen), achieving a recall at nearly 100%. This means that very capable of identifying all true TB positives, which is a primary need in clinical screening applications. The Adversarial Feature Selection used in the literature has value because it supports learning of robustly discriminative feature representation by allowing only clinically useful signals to be learned, by removing redundant information and selection of useful representations. This improves generalization, limits overfitting, and improves the global acceptance. Non-Local Wavelet de-noising improves input data collecting and provides more information with fewer features because it removes noise but preserves structure. This is important for making appropriate analyses on chest X-rays and other indications of how the solution is less sensitive to noise, which otherwise could create larger variation in the answer. The modified DenseNet architecture also provides useful results here in the sense of ensuring effective propagation of features and gradient flow between layers. The improved Adam optimizer allows for changes in learning rates more effectively, which leads to faster convergence and also helps stabilize the training. With the high recall walking backwards with the noise-tolerant, robust, sensitive solution, it has shown cross-dataset performance, and both are good options to rethink the feasibility of TB screening in the real world.

**4.18. Limitations**

While the development framework shows robust results, there are a few limitations. The study depended on only 2 total public datasets (Montgomery and Shenzhen) and therefore might not represent all real-world diversity in imaging conditions, demographics, and disease variants. In addition, the model in this study was limited to binary classification (TB versus Normal) and does not distinguish other pulmonary diseases that have overlapping characteristics. Even though the DL architecture demonstrated substantial accuracy, it requires significant computation and will need to be optimized or reduced in the number of calculations needed for low-power devices or real-time applications. In addition, as the model has not been externally validated nor has it undergone clinical trials, there is limited potential for its use in clinical practice at this time.

#### 4.19. Future Work

Future work will be carried out with a number of improvements to the detailed framework. First, it will be validated on different datasets like TBX11K and ChestX-ray14 to advance generalizability. Eventually, the framework will also be developed into a multi-class classification capable of distinguishing TB from pneumonia and lung cancer, and other thoracic diseases. Also, a study on model compression libraries and lightweight architectures will be researched for on-device and real-time and mobile deployments. Subsequently, the introduction of clinical metadata consisting of symptoms and/or patient history will also be pursued to continue making the models increasingly robust. Ultimately, the research and collaborate with healthcare providers for clinical trials in low-resource environments will successfully deploy the models.

### 5. Discussions

The framework achieves more effective detection of TB in images utilizing several components. First, the NLW algorithm needs to reduce the noise while preserving relevant image details to improve the learning of the features. Implemented Adversarial Feature Selection (AFS) to guarantee the model learns robust and discriminative features to improve the discrimination of the models, related to generalizing the models. The use of CNN-based segmentation will filter out unnecessary regions by focusing the models on the only relevant regions of the lung image and reducing the noise. The Modified Dense Architecture and improvement in the Adam Optimizer converged faster and improved the model

to not overfit. The results compared to the previous methods showed higher accuracy, precision, and recall when applied to two different datasets, Montgomery and Shenzhen. Overall, all of the component improvements produced a more accurate, robust, and efficient model to detect TB.

### 6. Conclusion

This research presents a thorough, hybrid DL framework for the automated identification of pulmonary TB from CXR images. The proposed method, by integrating NLW denoising, CNN-based segmentation, Adversarial Feature Selection, and a Modified DenseNet classifier supported with improved Adam optimization, can provide substantial gains in classification accuracy, sensitivity, and robustness. Detailed evaluation of the method on the Montgomery and Shenzhen datasets, along with ablation studies and statistical evaluations, provides the individual contributions of each module and evidence that the method's proposed performance gains are statistically significant. Not only does this model improve results over existing methods, but it does so with an important advantage in recall, thereby minimizing false negatives in TB diagnosis texts. Additionally, while there are limitations to this artwork - lack of external validation and the enormous computational demands - the framework has demonstrated strong potential for use in real-world environments for TB screening programs. Next steps for this project will be to consider/deliver multi-disease classification, deployment for mobile operation, and conducting prospective clinical validation trials in a variety of clinical practice settings.

### References

- [1] Tej Bahadur Chandra et al., "Automatic Detection of Tuberculosis-Related Abnormalities in Chest X-Ray Images using Hierarchical Feature Extraction Scheme," *Expert Systems with Applications*, vol. 158, 2020. [[CrossRef](#)] [[Google Scholar](#)] [[Publisher Link](#)]
- [2] Suliman Mohamed Fati, Ebrahim Mohammed Senan, and Narmine ElHakim, "Deep and Hybrid Learning Technique for Early Detection of Tuberculosis based on X-Ray Images using Feature Fusion," *Applied Sciences*, vol. 12, no. 14, pp. 1-23, 2022. [[CrossRef](#)] [[Google Scholar](#)] [[Publisher Link](#)]
- [3] Fatma Taher, and Naoufel Werghi, and Hussain Al-Ahmad, "Computer-Aided Diagnosis System for Early Lung Cancer Detection," *Algorithms*, vol. 8, no. 4, pp. 1088-1110, 2015. [[CrossRef](#)] [[Google Scholar](#)] [[Publisher Link](#)]
- [4] Sushil Ghildiyal, Saibal Manna and N. Ruban, "Layer-Based Deep Net Models for Automated Classification of Pulmonary Tuberculosis from Chest Radiographs," *International Journal of Medical Engineering and Informatics*, vol. 15, no. 1, pp. 58-69, 2023. [[CrossRef](#)] [[Google Scholar](#)] [[Publisher Link](#)]
- [5] Satyavratn Govindarajan, and Ramakrishnan Swaminathan, "Extreme Learning Machine-Based Differentiation of Pulmonary Tuberculosis in Chest Radiographs using Integrated Local Feature Descriptors," *Computer Methods and Programs in Biomedicine*, vol. 204, 2021. [[CrossRef](#)] [[Google Scholar](#)] [[Publisher Link](#)]
- [6] Rui Shen, Irene Cheng, and Anup Bas, "A Hybrid Knowledge-Guided Detection Technique for Screening of Infectious Pulmonary Tuberculosis from Chest Radiographs," *IEEE Transactions on Biomedical Engineering*, vol. 57, no. 11, pp. 2646-2656, 2010. [[CrossRef](#)] [[Google Scholar](#)] [[Publisher Link](#)]
- [7] Wei He et al., "Use of Low-Dose Computed Tomography to Assess Pulmonary Tuberculosis among Healthcare Workers in a Tuberculosis Hospital," *Infectious Diseases of Poverty*, vol. 6, no. 2, pp. 90-99, 2017. [[CrossRef](#)] [[Google Scholar](#)] [[Publisher Link](#)]
- [8] Li Wang et al., "Distinguishing Non-Tuberculous Mycobacteria from Mycobacterium Tuberculosis Lung Disease from CT Images using a Deep Learning Framework," *European Journal of Nuclear Medicine and Molecular Imaging*, vol. 48, no. 13, pp. 4293-4306, 2021. [[CrossRef](#)] [[Google Scholar](#)] [[Publisher Link](#)]
- [9] Jawad Rasheed, and Raed M. Shubair, "Screening Lung Diseases using Cascaded Feature Generation and Selection Strategies," *Healthcare*, vol. 10, no. 7, pp. 1-17, 2022. [[CrossRef](#)] [[Google Scholar](#)] [[Publisher Link](#)]

- [10] Chenggong Yan et al., “Cycle-Consistent Generative Adversarial Network: Effect on Radiation Dose Reduction and Image Quality Improvement in Ultralow-Dose CT for Evaluation of Pulmonary Tuberculosis,” *Korean Journal of Radiology*, vol. 22, no. 6, pp. 983-991, 2021. [[CrossRef](#)] [[Google Scholar](#)] [[Publisher Link](#)]
- [11] Xavier Alphonse Inbaraj et al., “A Novel Machine Learning Approach for Tuberculosis Segmentation and Prediction using Chest-X-Ray (CXR) Images,” *Applied Sciences*, vol. 11, no. 19, pp. 1-17, 2021. [[CrossRef](#)] [[Google Scholar](#)] [[Publisher Link](#)]
- [12] Kushagra Kushagra, Rajneesh Kumar, and Shaveta Jain, “A Deep Learning Model to Diagnose Lung Disease using Genetic Algorithm-Based Feature Selection Method,” *2022 4<sup>th</sup> International Conference on Advances in Computing, Communication Control and Networking (ICAC3N)*, Greater Noida, India, pp. 1251-1255, 2022. [[CrossRef](#)] [[Google Scholar](#)] [[Publisher Link](#)]
- [13] Paras Lakhani, and Baskaran Sundaram, “Deep Learning at Chest Radiography: Automated Classification of Pulmonary Tuberculosis by using Convolutional Neural Networks,” *Radiology*, vol. 284, no. 2, pp. 574-582, 2017. [[CrossRef](#)] [[Google Scholar](#)] [[Publisher Link](#)]
- [14] M.B. Mizan, M.A.M. Hasan, and S.R. Hassan, “A Comparative Study of Tuberculosis Detection using Deep Convolutional Neural Network,” *2020 2<sup>nd</sup> International Conference on Advanced Information and Communication Technology (ICAICT)*, Dhaka, Bangladesh, pp. 157-161, 2020. [[CrossRef](#)] [[Google Scholar](#)] [[Publisher Link](#)]
- [15] Shilpa Gite, Abhinav Mishra, and Ketan Kotecha, “Enhanced Lung Image Segmentation using Deep Learning,” *Neural Computing and Applications*, vol. 35, no. 31, pp. 22839-22853, 2023. [[CrossRef](#)] [[Google Scholar](#)] [[Publisher Link](#)]
- [16] Muhaza Liebenlito, Yanne Irene, and Abdul Hamid, “Classification of Tuberculosis and Pneumonia in Human Lung based on Chest X-Ray Image using Convolutional Neural Network,” *InPrime: Indonesian Journal of Pure and Applied Mathematics*, vol. 2, no. 1, pp. 24-32, 2020. [[CrossRef](#)] [[Google Scholar](#)] [[Publisher Link](#)]
- [17] Lanjuan Li, Haiyang Huang, and Xinyu Jin, “AE-CNN Classification of Pulmonary Tuberculosis based on CT Images,” *2018 9<sup>th</sup> International Conference on Information Technology in Medicine and Education (ITME)*, Hangzhou, China, pp. 39-42, 2018. [[CrossRef](#)] [[Google Scholar](#)] [[Publisher Link](#)]
- [18] Xinsen Zhou et al., “Enhanced Differential Evolution Algorithm for Feature Selection in Tuberculous Pleural Effusion Clinical Characteristics Analysis,” *Artificial Intelligence in Medicine*, vol. 153, 2024. [[CrossRef](#)] [[Google Scholar](#)] [[Publisher Link](#)]
- [19] Syed Kashif Badshah, and Noor Badshah, “Classification of Medical Images through Convolutional Neural Network Modification Method,” *International Journal of Innovations in Science & Technology*, vol. 6, no. 5, pp. 216-226, 2024. [[Google Scholar](#)] [[Publisher Link](#)]
- [20] Sugandha Agarwal, O.P. Singh, and Deepak Nagaria, “Analysis and Comparison of Wavelet Transforms for Denoising MRI Image,” *Biomedical and Pharmacology Journal*, vol. 10, no. 2, pp. 831-836, 2017. [[CrossRef](#)] [[Google Scholar](#)] [[Publisher Link](#)]
- [21] Muhammad Awais Malik et al., “A Novel Method for Lung Segmentation of Chest with Convolutional Neural Network,” *Prognostic Models in Healthcare: AI and Statistical Approaches*, Singapore, pp. 239-260, 2022. [[CrossRef](#)] [[Google Scholar](#)] [[Publisher Link](#)]
- [22] Ziming Wang et al., “Research on Computer-Aided Detection and Segmentation of Pulmonary Nodules based on Deep Learning and Generative Adversarial Networks,” *2020 IEEE 8<sup>th</sup> International Conference on Information, Communication and Networks (ICICN)*, Xi'an, China, pp. 172-176, 2020. [[CrossRef](#)] [[Google Scholar](#)] [[Publisher Link](#)]
- [23] Kartik Nair et al., “Analysing X-Ray Images to Detect Lung Diseases using DenseNet-169 Technique,” *Proceedings of the 7<sup>th</sup> International Conference on Innovations and Research in Technology and Engineering (ICIRTE-2022)*, Mumbai, India, 2022. [[CrossRef](#)] [[Google Scholar](#)] [[Publisher Link](#)]
- [24] Kanwarpartap Singh Gill et al., “Influence of Adam Optimizer with Sequential Convolutional Model for Detection of Tuberculosis,” *2022 International Conference on Computational Modelling, Simulation and Optimization (ICCMO)*, Pathum Thani, Thailand, pp. 340-344, 2022. [[CrossRef](#)] [[Google Scholar](#)] [[Publisher Link](#)]
- [25] Mostofa Ahsan, Rahul Gomes, and Anne Denton, “Application of a Convolutional Neural Network using Transfer Learning for Tuberculosis Detection,” *2019 IEEE International Conference on Electro Information Technology (EIT)*, Brookings, SD, USA, pp. 427-433, 2019. [[CrossRef](#)] [[Google Scholar](#)] [[Publisher Link](#)]
- [26] Hossein Arabi, and Habib Zaidi, “Spatially Guided Nonlocal Mean Approach for Denoising of PET Images,” *Medical Physics*, vol. 47, no. 4, pp. 1656-1669, 2020. [[CrossRef](#)] [[Google Scholar](#)] [[Publisher Link](#)]
- [27] Kapil Joshi et al., “Multi-Focus Image Fusion using Non-Local Mean Filtering and Stationary Wavelet Transform,” *International Journal of Innovative Technology and Exploring Engineering*, vol. 9, no. 1, pp. 344-350, 2019. [[CrossRef](#)] [[Google Scholar](#)] [[Publisher Link](#)]
- [28] Jinsol Ko, Soyeon Park, and Hyun Goo Woo, “Optimization of Vision Transformer-based Detection of Lung Diseases from Chest X-Ray Images,” *BMC Medical Informatics and Decision Making*, vol. 24, no. 1, pp. 1-8, 2024. [[CrossRef](#)] [[Google Scholar](#)] [[Publisher Link](#)]
- [29] Evans Kotei, and Ramkumar Thirunavukarasu, “Tuberculosis Detection from Chest X-Ray Image Modalities based on Transformer and Convolutional Neural Network,” *IEEE Access*, vol. 12, pp. 97417-97427, 2024. [[CrossRef](#)] [[Google Scholar](#)] [[Publisher Link](#)]
- [30] Jian Liu, and Yidi Huang, “Comparison of Different CNN Models in Tuberculosis Detecting,” *KSII Transactions on Internet and Information Systems (TIIS)*, vol. 14, no. 8, pp. 3519-3533, 2020. [[CrossRef](#)] [[Google Scholar](#)] [[Publisher Link](#)]
- [31] Latheesh Mangeri et al., “Chest Diseases Prediction from X-Ray Images using CNN Models: A Study,” *International Journal of Advanced Computer Science and Applications*, vol. 12, no. 10, pp. 236-243, 2021. [[CrossRef](#)] [[Google Scholar](#)] [[Publisher Link](#)]

- [32] Ahmed T. Sahlol et al., "A Novel Method for Detection of Tuberculosis in Chest Radiographs using Artificial Ecosystem-Based Optimisation of Deep Neural Network Features," *Symmetry*, vol. 12, no. 7, pp. 1-17, 2020. [[CrossRef](#)] [[Google Scholar](#)] [[Publisher Link](#)]
- [33] Ladislav Stanke et al., "Towards to Optimal Wavelet Denoising Scheme-A Novel Spatial and Volumetric Mapping of Wavelet-Based Biomedical Data Smoothing," *Sensors*, vol. 20, no. 18, pp. 1-24, 2020. [[CrossRef](#)] [[Google Scholar](#)] [[Publisher Link](#)]
- [34] Sergii Stirenko et al., "Chest X-Ray Analysis of Tuberculosis by Deep Learning with Segmentation and Augmentation," *2018 IEEE 38<sup>th</sup> International Conference on Electronics and Nanotechnology (ELNANO)*, Kyiv, Ukraine, pp. 422-428, 2018. [[CrossRef](#)] [[Google Scholar](#)] [[Publisher Link](#)]
- [35] S.N. Hankare, and S.S. Shirguppikar, *Detection of Tuberculosis and Lung Cancer using CNN*, Handbook of Smart Materials, Technologies, and Devices: Applications of Industry 4.0, Springer, pp. 1-11, 2021. [[CrossRef](#)] [[Google Scholar](#)] [[Publisher Link](#)]
- [36] Sahebgoud Hanamantray Karaddi, and Lakhan Dev Sharma, "Automated Multi-Class Classification of Lung Diseases from CXR-Images using Pre-Trained Convolutional Neural Networks," *Expert Systems with Applications*, vol. 211, 2023. [[CrossRef](#)] [[Google Scholar](#)] [[Publisher Link](#)]
- [37] N.B. Mahesh Kumar, K. Premalatha, and S. Suvitha, "Lung Disease detection using Self-Attention Generative Adversarial Capsule Network Optimized with Sunflower Optimization Algorithm," *Biomedical Signal Processing and Control*, vol. 79, 2023. [[CrossRef](#)] [[Google Scholar](#)] [[Publisher Link](#)]
- [38] Anup Pattnaik et al., "Predicting Tuberculosis Related Lung Deformities from CT Scan Images using 3D CNN," *CLEF (Working Notes)*, vol. 2380, pp. 1-16, 2019. [[Google Scholar](#)] [[Publisher Link](#)]
- [39] Aeri Rachmad, Nur Chamidah, and Riries Rulaningtyas, "Image Enhancement Sputum Containing Mycobacterium Tuberculosis using a Spatial Domain Filter," *IOP Conference Series: Materials Science and Engineering*, vol. 546, no. 5, pp. 1-8, 2019. [[CrossRef](#)] [[Google Scholar](#)] [[Publisher Link](#)]
- [40] Tawsifur Rahman et al., "Reliable Tuberculosis Detection using Chest X-Ray with Deep Learning, Segmentation and Visualization," *IEEE Access*, vol. 8, pp. 191586-191601, 2020. [[CrossRef](#)] [[Google Scholar](#)] [[Publisher Link](#)]
- [41] Jodh Singh et al., "Lung Tuberculosis Detection using Anti-Aliased Convolutional Networks," *Procedia Computer Science*, vol. 173, pp. 281-290, 2020. [[CrossRef](#)] [[Google Scholar](#)] [[Publisher Link](#)]
- [42] Marina Yusoff et al., "Tuberculosis X-Ray Images Classification based Dynamic Update Particle Swarm Optimization with CNN," *Journal of Human University Natural Sciences*, vol. 48, no. 9, pp. 504-514, 2021. [[Google Scholar](#)] [[Publisher Link](#)]
- [43] Ladan Ebadi et al., "A Review of Applying Second-Generation Wavelets for Noise Removal from Remote Sensing Data," *Environmental Earth Sciences*, vol. 70, no. 6, pp. 2679-2690, 2013. [[CrossRef](#)] [[Google Scholar](#)] [[Publisher Link](#)]
- [44] Ahmed Iqbal, Muhammad Usman, and Zohair Ahmed, "Tuberculosis Chest X-Ray Detection using CNN-Based Hybrid Segmentation and Classification Approach," *Biomedical Signal Processing and Control*, vol. 84, 2023. [[CrossRef](#)] [[Google Scholar](#)] [[Publisher Link](#)]
- [45] Geetamma Tummalapalli, Ch. Babji Prasad, and Jami Kousik, "Analysing the Performance of DenseNet in the Context of Tuberculosis Disease," *2024 International Conference on Advancements in Power, Communication and Intelligent Systems (APCI)*, Kannur, India, pp. 1-7, 2024. [[CrossRef](#)] [[Google Scholar](#)] [[Publisher Link](#)]
- [46] Wan Siti Halimatul Munirah Wan Ahmad, W. Mimi Diyana W. Zaki, and Mohammad Faizal Ahmad Fauzi, "Lung Segmentation on Standard and Mobile Chest Radiographs using Oriented Gaussian Derivatives Filter," *Biomedical Engineering Online*, vol. 14, no. 1, pp. 1-26, 2015. [[CrossRef](#)] [[Google Scholar](#)] [[Publisher Link](#)]
- [47] G. Geetha et al., "Multifocus Image Fusion using Multiresolution Approach with Bilateral Gradient based Sharpness Criterion," *Journal Computer Science & Information Technology*, vol. 10, pp. 103-115, 2012. [[CrossRef](#)] [[Google Scholar](#)] [[Publisher Link](#)]
- [48] Preena Prasad, and J. Anitha, "Non-Local Means Denoising of CT, MRI and US Images: An Investigation of Performance Under Varying Noise Levels," *1<sup>st</sup> International Conference on Recent Advancements in Computing Technologies & Engineering*, Ghaziabad, India, vol. 3168, no. 1, 2024. [[CrossRef](#)] [[Google Scholar](#)] [[Publisher Link](#)]
- [49] Prabhisek Singh, and Manoj Diwakar, "Wavelet-Based Multi-Focus Image Fusion using Average Method Noise Diffusion (AMND)," *Recent Advances in Computer Science and Communications*, vol. 14, no. 8, pp. 2436-2448, 2021. [[CrossRef](#)] [[Google Scholar](#)] [[Publisher Link](#)]
- [50] Eka Mala Sari Rochman, and Herry Suprajitno, "Comparison of Clustering in Tuberculosis using Fuzzy C-Means and k-Means Methods," *Communications in Mathematical Biology and Neuroscience*, vol. 2022, pp. 1-20, 2022. [[Google Scholar](#)] [[Publisher Link](#)]
- [51] Vinit Kumar Gunjan, Fahimuddin Shaik, and Amita Kashyap, "Detection and Analysis of Pulmonary TB using Bounding Box and K-Means Algorithm," *ICCCE 2020: Proceedings of the 3<sup>rd</sup> International Conference on Communications and Cyber Physical Engineering*, Singapore, pp. 1587-1595, 2020. [[CrossRef](#)] [[Google Scholar](#)] [[Publisher Link](#)]
- [52] Mengyang Zhao et al., "Faster Mean-Shift: GPU-Accelerated Clustering for Cosine Embedding-Based Cell Segmentation and Tracking," *Medical Image Analysis*, vol. 71, 2021. [[CrossRef](#)] [[Google Scholar](#)] [[Publisher Link](#)]
- [53] Sayali Abhijeet Salkade, and Sheetal Vikram Rathi, "An Adaptive Convolution Neural Network Model for Tuberculosis Detection and Diagnosis using Semantic Segmentation," *Polish Journal of Radiology*, vol. 90, pp. 124-137, 2025. [[CrossRef](#)] [[Google Scholar](#)] [[Publisher Link](#)]

- [54] Abidin Çalışkan, "Diagnosis of Malaria Disease by Integrating Chi-Square Feature Selection Algorithm with Convolutional Neural Networks and Autoencoder Network," *Transactions of the Institute of Measurement and Control*, vol. 45, no. 5, pp. 975-985, 2023. [[CrossRef](#)] [[Google Scholar](#)] [[Publisher Link](#)]
- [55] Szilárd Vajda et al., "Feature Selection for Automatic Tuberculosis Screening in Frontal Chest Radiographs," *Journal of Medical Systems*, vol. 42, no. 8, pp. 1-11, 2018. [[CrossRef](#)] [[Google Scholar](#)] [[Publisher Link](#)]
- [56] Khin Yadanar Win et al., "Hybrid Learning of Hand-Crafted and Deep-Activated Features using Particle Swarm Optimization and Optimized Support Vector Machine for Tuberculosis Screening," *Applied Sciences*, vol. 10, no. 17, pp. 1-12, 2020. [[CrossRef](#)] [[Google Scholar](#)] [[Publisher Link](#)]
- [57] Si-Yuan Lu et al., "CTBViT: A Novel ViT for Tuberculosis Classification with Efficient Block and Randomized Classifier," *Biomedical Signal Processing and Control*, vol. 100, pp. 1-9, 2025. [[CrossRef](#)] [[Google Scholar](#)] [[Publisher Link](#)]
- [58] Mamta Patankar, Vijayshri Chaurasia, and Madhu Shandilya, "EDenseNetViT: Leveraging Ensemble Vision Transform Integrated Transfer Learning for Advanced Differentiation and Severity Scoring of Tuberculosis," *International Journal of Imaging Systems and Technology*, vol. 35, no. 3, 2025. [[CrossRef](#)] [[Google Scholar](#)] [[Publisher Link](#)]
- [59] Benazeer Haque, Ebtasam Ahmad Siddiqui, and Abhinay Gupta, "Optimized Tuberculosis Image Classification in Chest X-Rays using Transfer Learning and Hyper Parameters," *2025 IEEE International Students' Conference on Electrical, Electronics and Computer Science (SCEECS)*, Bhopal, India, pp. 1-6, 2025. [[CrossRef](#)] [[Google Scholar](#)] [[Publisher Link](#)]